

## Smoothing algorithms for projected center-vortex gauge fields

Adam Virgili<sup>1</sup>, Waseem Kamleh<sup>1</sup>, and Derek Leinweber<sup>1</sup>

*Special Research Centre for the Subatomic Structure of Matter, Department of Physics,  
University of Adelaide, South Australia 5005, Australia*



(Received 23 March 2022; accepted 26 May 2022; published 11 July 2022)

We study the application of SU(3) gauge field smoothing methods to Z(3)-projected center-vortex gauge fields. Due to the proportionality of the vortex links to the identity, naive applications of these methods are either ineffectual or limited in scope, containing subtle issues that are not obviously manifest. To overcome these issues, we introduce *centrifuge preconditioning*, a novel method applied prior to smoothing that rotates the links away from the center while preserving the fundamental structure of the vortex field. Additionally, the concept of *vortex-preserved annealed smoothing* is formulated to ensure the smoothing procedure maintains the underlying vortex structure. The application of these new methods in the context of annealed smoothing applied to vortex fields is shown to successfully achieve the desired smoothness condition required for the study of more advanced operators.

DOI: 10.1103/PhysRevD.106.014505

### I. INTRODUCTION

Center vortices—topological structures of the QCD vacuum ground-state fields—are the prime candidate thought to underpin low-energy, nonperturbative QCD, in particular, its two key features: confinement and dynamical chiral symmetry breaking [1–26]. On the lattice, center vortices are revealed by projecting each gauge link to an element of the center  $Z(N)$  of SU( $N$ ), where

$$\begin{aligned} Z(N) &\equiv \{g \in \text{SU}(N) | gh = hg \ \forall \ h \in \text{SU}(N)\} \\ &= \{e^{i2\pi n/N} \mathbb{1} | n \in \mathbb{Z}_N\} \end{aligned} \quad (1)$$

is the set of elements in SU( $N$ ), which commute with every other element of the group. To obtain the center-projected links, the gauge field is fixed to maximal center gauge (MCG) by choosing the gauge transform  $U_\mu(x) \rightarrow U_\mu^G(x)$ , which maximizes the functional [27],

$$\sum_{x,\mu} |\text{Tr} U_\mu^G(x)|^2, \quad (2)$$

as outlined in Refs. [28,29]. Each link is then projected to the nearest element of  $Z(3)$ , such that

$$U_\mu^G(x) \rightarrow \mathcal{P}_{Z(3)}\{U_\mu^G(x)\} \equiv Z_\mu(x) = e^{i\frac{2\pi}{3}n_\mu(x)} \mathbb{1}, \quad (3)$$

where

$$n_\mu(x) = \begin{cases} 0, & \text{if } \arg \text{Tr} U_\mu^G(x) \in (-\frac{\pi}{3}, +\frac{\pi}{3}), \\ +1, & \text{if } \arg \text{Tr} U_\mu^G(x) \in (+\frac{\pi}{3}, +\pi), \\ -1, & \text{if } \arg \text{Tr} U_\mu^G(x) \in (-\pi, -\frac{\pi}{3}). \end{cases} \quad (4)$$

The projected links  $Z_\mu(x)$  define a center-vortex configuration in MCG. The elementary plaquette  $P_{\mu\nu}(x)$  is given by the product of links  $U$  around a unit square,

$$P_{\mu\nu}(x) = U_\mu(x)U_\nu(x + \hat{\mu})U_\mu^\dagger(x + \hat{\nu})U_\nu^\dagger(x). \quad (5)$$

Center vortices are identified by the vortex flux through each vortex-projected plaquette, where

$$\begin{aligned} P_{\mu\nu}(x) &= Z_\mu(x)Z_\nu(x + \hat{\mu})Z_\mu^\dagger(x + \hat{\nu})Z_\nu^\dagger(x) \\ &= e^{i\frac{2\pi}{3}p_{\mu\nu}(x)} \mathbb{1} \end{aligned} \quad (6)$$

corresponds to a vortex flux value  $p_{\mu\nu}(x) \in \{-1, 0, 1\}$ . A plaquette with vortex flux  $p_{\mu\nu}(x) = \pm 1$  is identified as pierced by a vortex with center charge  $\pm 1$ .

Composed only of links which are elements of  $Z(3)$ , projected center-vortex gauge fields are rough, and naturally, violate the smoothness condition of the overlap Dirac operator [30–33]. The vortex field must be smoothed. Previous pure-gauge center-vortex studies using overlap fermions [34,35] have employed cooling to this end. While cooling suffices for vortex fields derived from pure gauge backgrounds, it is not ideal for smoothing fields derived

Published by the American Physical Society under the terms of the [Creative Commons Attribution 4.0 International license](https://creativecommons.org/licenses/by/4.0/). Further distribution of this work must maintain attribution to the author(s) and the published article's title, journal citation, and DOI. Funded by SCOAP<sup>3</sup>.

from dynamical backgrounds. In the dynamical case, an ideal smoothing algorithm would not only be analytical, but also preserve the underlying vortex structure. The constrained cooling algorithm [36] gives an example of the importance of structure-preserving smoothing.

While there has been a successful, novel approach to smoothing  $Z(2)$  center-vortex gauge fields [37], this has not been generalized to  $Z(3)$ . As such, this work focuses on applying existing  $SU(3)$  gauge field smoothing algorithms to  $Z(3)$  center-vortex gauge fields, with the goal of smoothing the vortex field such that the smoothness condition of the overlap Dirac operator is satisfied.

Section II examines the behavior of analytic smoothing methods on vortex fields, specifically stout smearing, gradient flow, and APE-smearing with analytic projection. Section III looks at update-based smoothing, in particular the MaxReTr reuniterization process and its application to cooling and annealing. Section IV offers a novel preconditioning method—*centrifuge preconditioning*—for  $Z(3)$  center-vortex gauge fields as a solution to the shortfalls and limitations of the traditional smoothing algorithms encountered in the previous sections. Section V presents the results of the Wilson flow and annealed  $U$ -link smearing (AUS) [38] applied to a centrifuge preconditioned gauge field. Section VI introduces a vortex preservation step into the annealing process. Section VII compares three viable approaches to smoothing  $Z(3)$  center vortices arrived at over the course of the work presented herein. Section VIII summarizes the findings of this work.

## II. ANALYTIC SMOOTHING

When smoothing Monte Carlo generated gauge fields, the use of analytic smoothing methods is inherently desirable. There are a number of such methods, the most commonly used being stout link smearing [39] and the related gradient flow [40,41]. Through the use of a unitary projection method, it is also possible to apply APE-style blocking techniques while preserving analyticity [42]. The differentiability of such smoothing methods is advantageous as it means that they can be applied within the molecular dynamics integration component of the hybrid Monte Carlo algorithm [42,43]. More importantly, in the context of this work, the use of an analytic smoothing process implies that there is a parameterizable path within the gauge manifold that connects the original gauge links with the smoothed links.

The full  $SU(3)$  gauge group is described by eight real parameters, whereas the center group  $Z(3)$  consists of three discrete elements. The discrete nature of the center group presents significant challenges when attempting to apply standard smoothing techniques, as we demonstrate below. First, we define a quantity that is relevant to all the methods considered herein, namely the sum of the *staples* orthogonal to a link  $U_\mu(x)$ ,

$$\Sigma_\mu(x) = \sum_{\nu \neq \mu} [U_\nu(x)U_\mu(x + \hat{\nu})U_\nu^\dagger(x + \hat{\mu}) + U_\nu^\dagger(x - \hat{\nu})U_\mu(x - \hat{\nu})U_\nu(x - \hat{\nu} + \hat{\mu})]. \quad (7)$$

Related to the above, we also introduce the sum of the corresponding plaquettes (by closing the path of the staples via link multiplication) as

$$\Omega_\mu(x) = \Sigma_\mu(x)U_\mu^\dagger(x). \quad (8)$$

### A. Stout link smearing

Stout link smearing [39] provides the simplest case to show the difficulties of analytic smearing of center-vortex projected fields. A single iteration of stout link smearing with isotropic smearing parameter  $\rho$  is defined by

$$\tilde{U}_\mu(x) = \exp(\rho Q_\mu(x))U_\mu(x), \quad (9)$$

where  $Q_\mu(x)$  is the traceless anti-Hermitian projection of  $\Omega_\mu(x)$  onto the Lie algebra  $\mathfrak{su}(3)$ ,

$$Q_\mu(x) = \frac{1}{2}[\Omega_\mu(x) - \Omega_\mu^\dagger(x)] - \frac{1}{6}\text{Tr}[\Omega_\mu(x) - \Omega_\mu^\dagger(x)]. \quad (10)$$

In the case of a vortex field, as each of the center elements  $Z_\mu(x) \propto \mathbb{1}$  is proportional to the identity matrix, we can parameterize any sum of vortex link paths as  $re^{i\theta}\mathbb{1}$  where  $r, \theta \in \mathbb{R}$ . Consequently, we have that

$$Q_\mu(x) = \frac{1}{2}[re^{i\theta} - re^{-i\theta}]\mathbb{1} - \frac{1}{6}\text{Tr}[(re^{i\theta} - re^{-i\theta})\mathbb{1}]\mathbb{1} = 0. \quad (11)$$

As  $Q_\mu(x)$  vanishes when derived from a center-vortex field, it immediately follows from Eq. (9) that  $\tilde{U}_\mu(x) = U_\mu(x)$ . That is stout link smearing leaves the vortex field unchanged. This result remains true in the presence of a gauge transformation  $G(x)$ , as we have in general that

$$\Sigma_\mu(x) \rightarrow \Sigma_\mu^G(x) = G(x)\Sigma_\mu(x)G^\dagger(x + \hat{\mu}), \quad (12)$$

$$\Omega_\mu(x) \rightarrow \Omega_\mu^G(x) = G(x)\Omega_\mu(x)G^\dagger(x). \quad (13)$$

In the case of a vortex field, as the center group commutes with all other elements by definition, then we have that

$$\Omega_\mu^G(x) \rightarrow re^{i\theta}G(x)G^\dagger(x) = re^{i\theta}\mathbb{1}, \quad (14)$$

proving that a gauge transformed center-vortex field is also invariant under stout smearing.

### B. Gradient flow

The gradient flow [40,41] is defined by the equations,

$$\frac{d}{d\tau} U_\mu(x; \tau) = Q_\mu(x)[U(\tau)]U_\mu(x; \tau), \quad (15)$$

$$U_\mu(x; 0) = U_\mu(x), \quad (16)$$

where  $\tau$  is dimensionless *flow time*, and  $Q_\mu(x)[U(\tau)] \in \mathfrak{su}(3)$  is the generator of the infinitesimal field transformation,

$$U \rightarrow U + \epsilon Q(U)U + \mathcal{O}(\epsilon^2). \quad (17)$$

In particular, the *Wilson flow* is generated by

$$Q_\mu(x)[U] = T^a \partial_{x,\mu}^a \sum_{x,\mu \neq \nu} \text{Tr}[P_{\mu\nu}(x)[U]], \quad (18)$$

where  $T^a$  are the generators of SU(3) (see Appendix A), and

$$\partial_{x,\mu}^a f(U) = \left. \frac{d}{ds} f(e^{sX^a} U) \right|_{s=0}, \quad (19)$$

$$X^a(y, \nu) = \begin{cases} T^a & \text{if } (y, \nu) = (x, \mu) \\ 0 & \text{otherwise.} \end{cases} \quad (20)$$

The explicit formula for the generator  $Q_\mu(x)[U]$  is identical to that for stout smearing given in Eq. (10). In fact, noting that

$$\lim_{n \rightarrow \infty} (1 + \epsilon Q)^n U = \exp(\epsilon Q)U, \quad (21)$$

we can map  $\epsilon \rightarrow \rho$  and see that the stout-smear link is the finite transformation generated by the Wilson flow process for sufficiently small smearing parameters.

It trivially follows that for a center-vortex field  $U_\mu(x; 0) = Z_\mu(x)$ , we have

$$\frac{d}{d\tau} U_\mu(x; \tau) = 0 \quad \forall x, \mu, \tau. \quad (22)$$

Hence, independent of the initial gauge or the integration method, the Wilson flow of a center-vortex gauge field is invariant.

### C. APE smearing with analytic projection

We now consider APE smearing [44,45] with the analytic projection method defined in Ref. [42], which we refer to as *unit circle projection*. The APE smearing process starts with a blocking step, where the original link  $U_\mu(x)$  is mixed with the sum of the staples in proportion to the smearing parameter  $\alpha$  to define the blocked matrix,

$$V[U_\mu(x)] \equiv V_\mu(x) = (1 - \alpha)U_\mu(x) + \frac{\alpha}{6}\Sigma_\mu(x). \quad (23)$$

This construction of  $V_\mu(x)$  is gauge equivariant, which is to say, under a gauge transformation,

$$U_\mu(x) \rightarrow U_\mu^G(x) = G(x)U_\mu(x)G^\dagger(x + \hat{\mu}), \quad (24)$$

that

$$V[U_\mu^G(x)] = G(x)V[U_\mu(x)]G^\dagger(x + \hat{\mu}). \quad (25)$$

Setting  $U_\mu^{(0)}(x) = U_\mu(x)$ , the APE smearing update is then defined by

$$U_\mu^{(n)}(x) \rightarrow U_\mu^{(n+1)}(x) = \mathcal{P}\{V_\mu^{(n)}(x)\}, \quad (26)$$

where the blocked matrix  $V_\mu^{(n)}(x) \equiv V[U_\mu^{(n)}(x)] \notin \text{SU}(3)$  must be returned back to the gauge group. This may be performed in an analytic manner by first performing a unitary projection,

$$W_\mu(x) = V_\mu(x) \frac{1}{\sqrt{V_\mu^\dagger(x)V_\mu(x)}}, \quad (27)$$

such that the eigenvalues of  $W$  lie on the unit circle. The final step in the unit circle projection is multiplying by the appropriate phase in order to return to SU(3),

$$\mathcal{P}_{\text{ucp}}\{V_\mu(x)\} = \frac{1}{\sqrt[3]{\det W_\mu(x)}} W_\mu(x). \quad (28)$$

As shown in Ref. [42], the unit circle projection is gauge equivariant such that the smeared links share the same gauge transformation properties as the original link,

$$U_\mu^{(n)}(x) \rightarrow G(x)U_\mu^{(n)}(x)G^\dagger(x + \hat{\mu}). \quad (29)$$

In standard APE smearing, the staples term  $\Sigma_\mu(x)$  is defined as per Eq. (7), but other choices are possible, in particular, the overimprovement formalism [46–48] outlined in Eq. (53). For the purposes of the following discussion, we generalize  $\Sigma_\mu(x)$  to sum over any combination of operators constructed from paths originating at lattice site  $x$  and terminating at  $x + \hat{\mu}$ .

When APE smearing is applied to a center-vortex gauge field in an arbitrary gauge [noting that  $Z_\mu(x) \propto \mathbb{1}$ ], we can use gauge equivariance to write

$$V_\mu^{(0)}(x) = r e^{i\theta} G(x)G^\dagger(x + \hat{\mu}). \quad (30)$$

Applying the unitary projection in Eq. (27) gives

$$\begin{aligned} W_\mu(x) &= r e^{i\theta} G(x) G^\dagger(x + \hat{\mu}) \frac{\mathbb{1}}{\sqrt{r^2}} \\ &= e^{i\theta} G(x) G^\dagger(x + \hat{\mu}). \end{aligned} \quad (31)$$

Noting that  $\det W_\mu(x) = e^{i3\theta}$ , we have that

$$\sqrt[3]{\det W_\mu(x)} = e^{i(\theta + \frac{2k\pi}{3})}, \quad (32)$$

where  $k \in \{0, 1, 2\}$  is chosen to correspond to the principal cube root, i.e., such that

$$-\frac{\pi}{3} < \theta + \frac{2k\pi}{3} < \frac{\pi}{3}. \quad (33)$$

Hence, the projected link is given by

$$\begin{aligned} Z_\mu^{(1)}(x) &= \frac{1}{e^{i(\theta + \frac{2k\pi}{3})}} e^{i\theta} G(x) G^\dagger(x + \hat{\mu}) \\ &= e^{-i\frac{2k\pi}{3}} G(x) G^\dagger(x + \hat{\mu}), \end{aligned} \quad (34)$$

where  $e^{-i\frac{2k\pi}{3}} \mathbb{1} \in Z(3)$ .

The key result here is that it is only possible to project to another element of  $Z(3)$ . That is, applying APE smearing with unit circle projection to a vortex link results in either the original link remaining unchanged or selecting a completely different center element and thereby radically altering the vortex structure such that it no longer resembles its original form. As the method is gauge equivariant, this is true regardless of whether we are in maximal center gauge or not.

### III. UPDATE-BASED SMOOTHING

Having determined that none of the analytic smearing techniques considered above can smoothly deform a vortex field away from the center group, we consider a nonanalytic alternative. Specifically, we examine APE-style blocking coupled with the update-based reunitization method, maximizing the real part of the trace (MaxReTr) of the plaquette. This process is based on the Cabibbo-Marinari pseudo-heat-bath algorithm [49], which iteratively updates a candidate  $SU(N)$  matrix  $U_\mu(x)$  to maximize the following:

$$\max \text{Re Tr}[U_\mu(x) V_\mu^\dagger(x)], \quad (35)$$

where  $V_\mu(x)$  is the sum of link paths defined in Eq. (23). MaxReTr reunitization is fundamentally connected with cooling [47], as if we set the smearing fraction  $\alpha = 1$ , then we have  $V_\mu(x) \propto \Sigma_\mu(x)$  and then the MaxReTr update selects the link which minimizes the local action in a way that does not depend on the original link.

Due to the nonanalytic nature of the MaxReTr update process, it is able to shift the vortex fields away from the

center group in a way that the differentiable smoothing methods above cannot. It will prove useful to review the specific details of the MaxReTr method as applied to  $SU(3)$ , which involves iterating over  $SU(2)$  subgroups in order to achieve the optimization specified by Eq. (35). First, define the matrix  $L^1$  by

$$L^1 = U_\mu(x) V_\mu^\dagger(x). \quad (36)$$

From  $L^1$ , another matrix,  $T_1 \in SU(2) \subset SU(3)$ , given by

$$T_1 = \frac{1}{2} \begin{bmatrix} L_{11}^1 + (L_{22}^1)^* & L_{12}^1 - (L_{21}^1)^* & 0 \\ L_{21}^1 - (L_{12}^1)^* & (L_{11}^1)^* + L_{22}^1 & 0 \\ 0 & 0 & 2 \end{bmatrix}, \quad (37)$$

is constructed, where  $L_{ij}^1$  is element  $(i, j)$  of  $L^1$ . Setting  $k = \sqrt{\det T_1}$ , this matrix is cooled such that

$$[T_1^c]_{2 \times 2} = \frac{1}{k} [T_1^\dagger]_{2 \times 2} \in SU(2), \quad (38)$$

within the embedded  $2 \times 2$  subgroup, and the full matrix  $T_1^c$  is the embedding of the resulting submatrix into  $SU(3)$ . The original link is then updated by

$$U_\mu(x) \rightarrow U'_\mu(x) = T_1^c U_\mu(x). \quad (39)$$

This process is typically repeated for the other two diagonal  $SU(2)$  subgroups, which together, comprehensively cover  $SU(3)$ , such that

$$L^2 = U'_\mu(x) V_\mu^\dagger(x) = T_1^c U_\mu(x) V_\mu^\dagger(x), \quad (40)$$

$$L^3 = U''_\mu(x) V_\mu^\dagger(x) = T_2^c T_1^c U_\mu(x) V_\mu^\dagger(x), \quad (41)$$

and

$$T_2 = \frac{1}{2} \begin{bmatrix} 2 & 0 & 0 \\ 0 & L_{22}^2 + (L_{33}^2)^* & L_{23}^2 - (L_{32}^2)^* \\ 0 & L_{32}^2 - (L_{23}^2)^* & (L_{22}^2)^* + L_{33}^2 \end{bmatrix}, \quad (42)$$

$$T_3 = \frac{1}{2} \begin{bmatrix} L_{11}^3 + (L_{33}^3)^* & 0 & L_{13}^3 - (L_{31}^3)^* \\ 0 & 2 & 0 \\ L_{31}^3 - (L_{13}^3)^* & 0 & (L_{11}^3)^* + L_{33}^3 \end{bmatrix}. \quad (43)$$

The updated link  $U_\mu^{(1)}(x)$  after one loop over the  $SU(2)$  subgroups is given by

$$T_3^c T_2^c T_1^c U_\mu(x). \quad (44)$$

In principle, one loop over the subgroups is considered sufficient with regard to approaching the maximum defined



by Eq. (35). Here, we choose to perform three iterations over the subgroups as multiple loops provide an advantage in converging to the optimal link [47].

Let us now explore how the MaxReTr renitization algorithm applies to a center-vortex gauge field that has undergone an arbitrary gauge transformation,

$$Z_\mu(x) \rightarrow G(x)Z_\mu(x)G^\dagger(x + \hat{\mu}). \quad (45)$$

Using the gauge equivariance of  $V_\mu(x)$ ,  $L^1$  has the gauge invariant form,

$$\begin{aligned} L^1 &= G(x)Z_\mu(x)G^\dagger(x + \hat{\mu})G(x + \hat{\mu})V_\mu^\dagger(x)G^\dagger(x) \\ &= G(x)re^{i(\frac{2\pi n}{3} - \theta)}G^\dagger(x) \\ &\equiv re^{i\phi}\mathbb{1}, \end{aligned} \quad (46)$$

where  $V_\mu(x) = re^{i\theta}$  is in MCG, and we have defined  $\phi \equiv \frac{2\pi n}{3} - \theta$  for  $Z_\mu(x) = e^{i\frac{2\pi n}{3}}\mathbb{1}$  also in MCG. Hence,  $T_1$  is given by

$$\begin{aligned} T_1 &= \frac{1}{2} \begin{bmatrix} r(e^{i\phi} + e^{-i\phi}) & 0 & 0 \\ 0 & r(e^{i\phi} + e^{-i\phi}) & 0 \\ 0 & 0 & 2 \end{bmatrix} \\ &= \begin{bmatrix} r \cos \phi & 0 & 0 \\ 0 & r \cos \phi & 0 \\ 0 & 0 & 1 \end{bmatrix}. \end{aligned} \quad (47)$$

It follows then that

$$k = \sqrt{\det T_1} = \sqrt{r^2 \cos^2 \phi} = |r \cos \phi|, \quad (48)$$

and

$$T_1^c = \begin{bmatrix} \text{sgn}(r \cos \phi) & 0 & 0 \\ 0 & \text{sgn}(r \cos \phi) & 0 \\ 0 & 0 & 1 \end{bmatrix}. \quad (49)$$

If  $r \cos \phi > 0 \Rightarrow T_1^c = \mathbb{1}$  and

$$Z'_\mu(x) = T_1^c Z_\mu(x) = Z_\mu(x), \quad (50)$$

it is straightforward to see that  $T_1^c = \mathbb{1} \Rightarrow T_i^c = \mathbb{1} \ \forall i$ , and hence,

$$Z_\mu^{(1)}(x) = Z_\mu(x). \quad (51)$$

By induction,

$$Z_\mu^{(n)}(x) = Z_\mu(x) \quad \forall n, \quad (52)$$

and the center-vortex field is unchanged.

As such, in order to perturb the vortex field, we require  $r \cos \phi < 0$ , or equivalently,  $|\phi| > \frac{\pi}{2}$ . This necessarily places a condition on the smearing parameter  $\alpha$ . We consider this condition within the context of the overimprovement formalism [48], for which the staples term is given by the diagrammatic equation,

$$\Sigma_\mu^\dagger(x) = \sum_{\nu \neq \mu} \frac{5 - 2\epsilon}{3} \left( \begin{array}{c} \text{---} \circ \text{---} \\ \uparrow \quad \downarrow \\ \text{---} \circ \text{---} \end{array} + \begin{array}{c} \text{---} \circ \text{---} \\ \downarrow \quad \uparrow \\ \text{---} \circ \text{---} \end{array} \right) + \frac{\epsilon - 1}{12u_0^2} \left( \begin{array}{c} \text{---} \circ \text{---} \\ \uparrow \quad \downarrow \\ \text{---} \circ \text{---} \end{array} + \begin{array}{c} \text{---} \circ \text{---} \\ \downarrow \quad \uparrow \\ \text{---} \circ \text{---} \end{array} + \begin{array}{c} \text{---} \circ \text{---} \\ \uparrow \quad \downarrow \\ \text{---} \circ \text{---} \end{array} + \begin{array}{c} \text{---} \circ \text{---} \\ \downarrow \quad \uparrow \\ \text{---} \circ \text{---} \end{array} + \begin{array}{c} \text{---} \circ \text{---} \\ \uparrow \quad \downarrow \\ \text{---} \circ \text{---} \end{array} + \begin{array}{c} \text{---} \circ \text{---} \\ \downarrow \quad \uparrow \\ \text{---} \circ \text{---} \end{array} \right), \quad (53)$$

where the solid dot represents the point  $x$ , the open dot represents the point  $x + \hat{\mu}$ , and the links in the positive orthogonal direction  $\hat{\nu}$  are shown as pointing vertically up the page. Note also that we have illustrated the link paths as oriented for the Hermitian conjugate  $\Sigma_\mu^\dagger(x)$  which enters into Eq. (35).

The overimprovement formalism encapsulates standard APE smearing at overimprovement term  $\epsilon = 1$ . To ensure  $r \cos \phi < 0$ , we require that

$$\alpha > \alpha_{\min} = \frac{-6}{2\epsilon - 11 + \frac{3}{2}(\frac{\epsilon-1}{u_0^2})}, \quad (54)$$

for  $\epsilon \in [-\frac{5}{2}, 1]$ , where  $u_0$  is the mean link. See Appendix B for a derivation.

In Fig. 1, all possible values of  $re^{i\phi}$  originating from a center-vortex configuration for  $\epsilon = -0.25$  and  $u_0 = 1$ , at  $\alpha = 0.4$  and  $\alpha = 0.7$ , respectively, are plotted on the complex plane. At  $\alpha = 0.7$ , there are many combinations of links which yield  $|\phi| > \frac{\pi}{2}$ , but none at  $\alpha = 0.4$ . In fact, from Eq. (54),  $\alpha_{\min}(\epsilon = -0.25, u_0 = 1) \approx 0.4486$ . Of course, this is the limit to have *any* combination of links yield  $|\phi| > \frac{\pi}{2}$ . In a practical sense, we require something more like  $\alpha > 0.6$  to achieve effective smearing.

Figure 2 presents the proportion  $p_{\text{in}}$  of link combinations for which  $|\phi| > \frac{\pi}{2}$  in the  $\beta \rightarrow 0$  limit where each link in the construction of  $L^1$  has an equal probability to be one of the center phase elements. Each combination is weighted by its multiplicity. These do not reflect the true probabilities that would be encountered on an actual Z(3) center-vortex gauge field but suffice for demonstrative purposes.

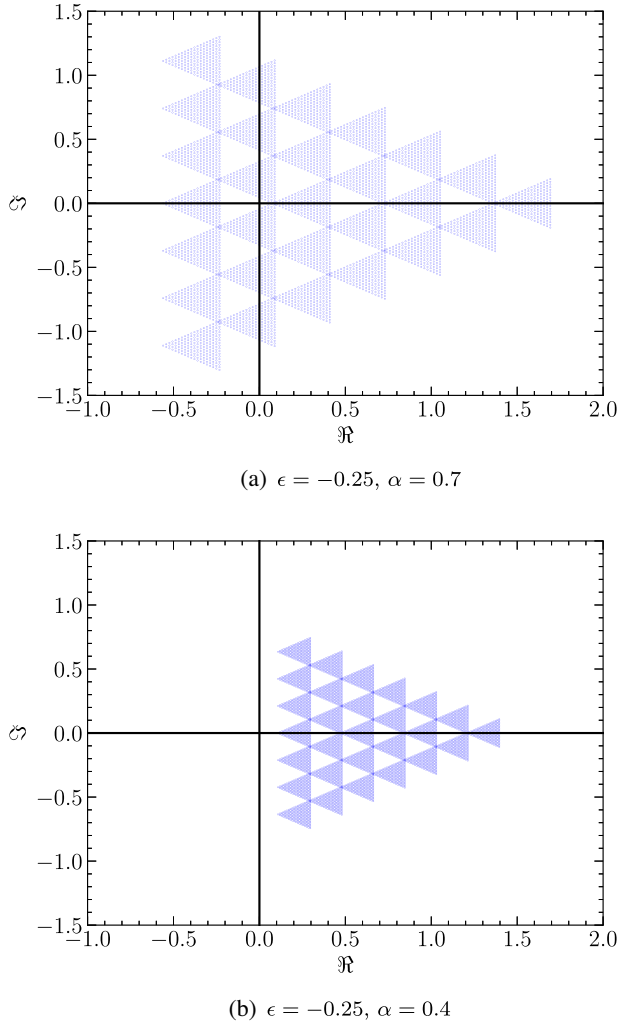


FIG. 1. The complex plane showing all possible values of  $re^{i\phi}$  for overimprovement term  $\epsilon = -0.25$  at smearing parameters (a)  $\alpha = 0.7$  and (b)  $\alpha = 0.4$ .

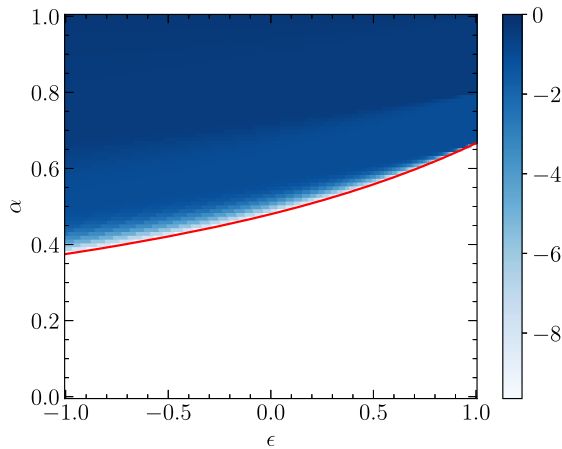


FIG. 2.  $\log_{10}(p_{in})$  as a function of  $\epsilon$  and  $\alpha$ , at  $u_0 = 1$  fixed in the limit  $\beta \rightarrow 0$ . The shaded region illustrates the admissible values of  $\alpha$  and  $\epsilon$  where the proportion of acceptable link combinations,  $p_{in}$ , exceeds zero. The red line is  $\alpha_{min}(\epsilon)$ .

### A. Cooling and annealing

While smearing algorithms update all links simultaneously, smoothing via a cooling or annealing process updates each link individually. These updates can be done in parallel with appropriate masking so as to preserve the validity of the cooling or annealing process [50]. The Wilson flow can be considered as an annealed version of stout link smearing with small smearing parameter. *Annealed U-link smearing* (AUS) [38] is similarly related to APE smearing in that the update process uses APE-style blocking and reunitarization but applied to individual links rather than all links. In particular, at  $\alpha = 1.0$ , the form of AUS with MaxReTr reunitarization at the individual link level reduces to that of cooling [51–55]—up to choice of operators in the staples term.

Our analysis with regard to vortex smoothing above extends to the annealed form of the various methods and also to cooling in the special case of  $\alpha = 1.0$ . With regard to cooling, it should be noted that it is possible to encounter some numerical issues when smoothing center-vortex fields. From Eqs. (36) and (46), we can write  $L^1$  in arbitrary gauge as

$$L^1 = (1 - \alpha) + \frac{\alpha}{6} Z_\mu(x) \Sigma_\mu^\dagger(x), \quad (55)$$

which reduces to

$$L^1 = \frac{1}{6} Z_\mu(x) \Sigma_\mu^\dagger(x) \quad (56)$$

for cooling ( $\alpha = 1.0$ ), where  $Z_\mu(x)$  and  $\Sigma_\mu(x)$  are in MCG; i.e., they are proportional to  $\mathbb{1}$ .

Since  $\Sigma_\mu(x)$  is a sum of elements of  $Z(3)$ , each multiplied by some real factor, there exists combinations of links for which  $\Sigma_\mu(x) = is\mathbb{1}$  and  $s \in \mathbb{R}$ , which is to say that the nonzero (diagonal) elements of  $\Sigma_\mu(x)$  are purely imaginary. For example, consider the six operators comprising the staples term in standard Wilson cooling. In the cases where these operators are split two-to-four between  $I$  and  $e^{\pm i\frac{2\pi}{3}}$ , the staples term is given by

$$\Sigma_\mu(x) = 2\mathbb{1} + 4e^{\pm i\frac{2\pi}{3}} = is \approx \pm i3.464\dots \quad (57)$$

Without loss of generality, choose  $Z_\mu(x) = \mathbb{1}$ . Then

$$\begin{aligned} L^1 &= Z_\mu(x) V_\mu^\dagger(x) \\ &= \begin{bmatrix} -is & 0 & 0 \\ 0 & -is & 0 \\ 0 & 0 & -is \end{bmatrix}. \end{aligned} \quad (58)$$

Constructing  $T_1$  according to Eq. (37),

TABLE I. The number of links of a  $Z(3)$  pure gauge field configuration satisfying various conditions.  $n_{\text{in}}$  counts the links that satisfy  $|\phi| > \frac{\pi}{2}$ .  $n_{\text{diff}}$  counts the links for which  $Z_{\mu}^{(1)}(x) \neq Z_{\mu}(x)$ .  $n_{\text{pass}}$  counts the links satisfying the preservation condition given  $Z_{\mu}^{(1)}(x) \neq Z_{\mu}(x)$ . The  $20^3 \times 40$  lattice has 1,280,000 links.

$\alpha$	$n_{\text{in}}$	$n_{\text{diff}}$	$n_{\text{pass}}$
0.4	0	0	0
0.5	0	0	0
0.6	527	527	0
0.7	535	535	0
0.8	1635	1635	0
0.9	1636	1636	0
1.0	4570	4582	0

$$T_1 = \frac{1}{2} \begin{bmatrix} -is + is & 0 & 0 \\ 0 & +is - is & 0 \\ 0 & 0 & 2 \end{bmatrix} = \begin{bmatrix} 0 & 0 & 0 \\ 0 & 0 & 0 \\ 0 & 0 & 1 \end{bmatrix}, \quad (59)$$

which implies  $k = \sqrt{\det T_1} = 0$ , and thus,

$$[T_1^c]_{2 \times 2} = \frac{1}{k} [T_1^\dagger]_{2 \times 2}, \quad (60)$$

is undefined.

In practice, the diagonal elements of  $T_1$  are not precisely 0 due to floating-point artifacts. From these artifacts, the algorithm is able to generate an essentially random  $SU(3)$  link without breaking or resulting in any obvious errors. This is apparent in Table I, where at  $\alpha = 1.0$ , the number of links for which  $Z_{\mu}^{(1)}(x) \neq Z_{\mu}(x)$ ,  $n_{\text{diff}}$ , is greater than  $n_{\text{in}}$ , the number of links for which  $|\phi| > \frac{\pi}{2}$ . While this situation is rare (12 of 1,280,000 links in Table I), the link, generated essentially from random noise, contaminates neighboring links on the next iteration when it contributes to the staples term. The noise contamination continues to propagate throughout the lattice after each successive sweep, as the contaminated neighbors then contaminate their neighbors.

#### IV. CENTRIFUGE PRECONDITIONING

The issues and limitations, outlined in previous sections, which arise when applying traditional smoothing methods to center-vortex gauge fields, are all, at root, due to the proportionality of the links to the identity. As such, we introduce a method to break this symmetry without altering the fundamental vortex structure of the field. The key idea is to rotate the vortex links away from the center elements

before applying smoothing, and hence, we call this new method *centrifuge preconditioning*.

We start with the original center-vortex gauge field in MCG and denote

$$Z_{\mu}(x) = \begin{bmatrix} e^{i\lambda_{\mu}^1(x)} & 0 & 0 \\ 0 & e^{i\lambda_{\mu}^2(x)} & 0 \\ 0 & 0 & e^{i\lambda_{\mu}^3(x)} \end{bmatrix}, \quad (61)$$

where initially the diagonal entries  $\lambda_{\mu}^i(x) = \lambda_{\mu}(x)$  are all equal. Noting that we are now within the diagonal subgroup of  $SU(3)$ , which is isomorphic to  $U(1) \times U(1) \times Z(3)$ , we can work with the phases directly in the noncompact representation. Define the staple phase as

$$\sigma_{\mu}(x) = \frac{1}{6} \sum_{\nu \neq \mu} [\lambda_{\nu}(x) + \lambda_{\mu}(x + \hat{\nu}) - \lambda_{\nu}(x + \hat{\mu}) - \lambda_{\nu}(x - \hat{\nu}) + \lambda_{\mu}(x - \hat{\nu}) + \lambda_{\nu}(x - \hat{\nu} + \hat{\mu})]. \quad (62)$$

A pair of indices  $(j, k) \in \{(1, 2), (2, 3), (3, 1)\}$  are selected randomly for each link, and then the corresponding phases of each original link are updated according to

$$\lambda_{\mu}^j(x) \rightarrow (1 - \omega)\lambda_{\mu}(x) + \omega\sigma_{\mu}(x), \quad (63)$$

$$\lambda_{\mu}^k(x) \rightarrow (1 + \omega)\lambda_{\mu}(x) - \omega\sigma_{\mu}(x), \quad (64)$$

where  $\omega \in \mathbb{R}$  specifies the *centrifugal rotation angle*, noting that the centrifuge update above corresponds to a phase rotation by  $\mp \omega(\lambda - \sigma)$ . This leaves the sum of the three phases invariant. Hence, as the sum of the three phases of each center element is distinct,

$$\sum_j \lambda_{\mu}^j(x) = n2\pi, \quad n \in \{-1, 0, 1\}, \quad (65)$$

after centrifuge preconditioning, it is possible to uniquely identify the original center element by this sum.

#### A. Preservation of vortex structure

Recall from Eqs. (3) and (4) that the center-vortex links are obtained by projecting the untouched link in maximal center gauge  $U_{\mu}^G(x)$  to the center element with phase nearest to  $\arg \text{Tr} U_{\mu}^G(x)$ . Since we seek to break the diagonal symmetry of the center-vortex links in such a way that preserves the underlying vortex structure, we restrict  $\omega$  in Eqs. (63) and (64) such that  $\arg \text{Tr} Z_{\mu}(x) = 2\pi n_{\mu}(x)/3$  is preserved.

Let  $Z'_{\mu}(x)$  denote the preconditioned center-vortex link with updated phases  $\lambda_{\mu}^j(x)$  and  $\lambda_{\mu}^k(x)$ . It is simple to see that

$$\text{Tr}[Z'_{\mu}(x)] = e^{i\lambda_{\mu}^j(x)} + e^{i\lambda_{\mu}^k(x)} + e^{i\frac{2\pi n_{\mu}}{3}}. \quad (66)$$

We then define

$$\Lambda^\pm = \frac{1}{2}(\lambda_\mu^j(x) \pm \lambda_\mu^k(x)). \quad (67)$$

Utilizing polar form  $e^{iA} = \cos A + i \sin A$ , and the following trigonometric properties,

$$\cos A + \cos B = 2 \cos \frac{A+B}{2} \cos \frac{A-B}{2}, \quad (68)$$

$$\sin A + \sin B = 2 \sin \frac{A+B}{2} \cos \frac{A-B}{2}, \quad (69)$$

we obtain

$$\begin{aligned} e^{i\lambda_\mu^j(x)} + e^{i\lambda_\mu^k(x)} &= 2 \cos \Lambda^+ \cos \Lambda^- + i2 \sin \Lambda^+ \cos \Lambda^- \\ &= 2 \cos \Lambda^- (\cos \Lambda^+ - i \sin \Lambda^+) \\ &= 2 \cos \Lambda^- e^{i\frac{2\pi}{3}}. \end{aligned} \quad (70)$$

Hence,

$$\text{Tr}[Z'_\mu(x)] = (2 \cos \Lambda^- + 1)e^{n\frac{2\pi}{3}}, \quad (71)$$

and the phase of the trace is preserved,

$$\arg \text{Tr}[Z_\mu(x)] = \arg \text{Tr}[Z'_\mu(x)] = n2\pi/3, \quad (72)$$

provided

$$2 \cos \Lambda^- + 1 > 0. \quad (73)$$

For the above condition to hold, we must have

$$-\frac{2\pi}{3} < \Lambda^- < \frac{2\pi}{3}. \quad (74)$$

Explicitly, this implies that

$$-\frac{2\pi}{3} < \omega[\sigma_\mu(x) - \lambda_\mu(x)] < \frac{2\pi}{3}, \quad (75)$$

where we have used Eqs. (63) and (64). Since

$$\lambda_\mu(x) = n \frac{2\pi}{3}, \quad n \in \{-1, 0, 1\}, \quad (76)$$

$$\sigma_\mu(x) = m \frac{2\pi}{6 \cdot 3}, \quad m \in [-18, 18] \subset \mathbb{Z}, \quad (77)$$

we can rewrite Eq. (75) as

$$-\frac{2\pi}{3} < \omega \left[ m \frac{2\pi}{6 \cdot 3} - n \frac{2\pi}{3} \right] < \frac{2\pi}{3}, \quad (78)$$

which, for  $\omega > 0$ , simplifies to

$$\omega|m - 6n| < 6. \quad (79)$$

Considering the extrema where  $m = \pm 18$  and  $n = \mp 1$ , we require that

$$\omega < \frac{1}{4}. \quad (80)$$

In practice, we always choose small  $\omega \ll \frac{1}{4}$ .

## V. CENTRIFUGE PRECONDITIONED SMOOTHING

We consider a center-vortex configuration projected from a  $20^3 \times 40$  Luscher-Weisz  $\mathcal{O}(a^2)$  mean-field-improved action pure-gauge configuration with lattice spacing  $a = 0.125$  fm. This same configuration is used throughout the rest of the paper. It is expected that the total action will increase after the vortex links have experienced centrifuge preconditioning. In general, we desire the centrifugal rotation angle  $\omega$  to be small as we only wish to minimally perturb the vortex links.

In Figs. 3 and 4 the action density  $S(x)$  and topological charge density  $q(x)$  of the center-vortex gauge field are compared before and after the centrifuge preconditioning at  $\omega = 0.02$  has been applied. This value of  $\omega$  was chosen to sufficiently rotate the links away from the center while keeping the increase in the total action to an acceptable level. Shown are the standard Wilson action density,

$$S(x) = \frac{\beta}{2n_c n_d (n_d - 1)} \sum_{\substack{\mu, \nu \\ \mu \neq \nu}} \text{Re Tr}[1 - P_{\mu\nu}(x)], \quad (81)$$

and the one-loop topological charge density,

$$q(x) = \frac{1}{32\pi^2} \epsilon_{\mu\nu\rho\sigma} \text{Tr}[F^{\mu\nu}(x)F^{\rho\sigma}], \quad (82)$$

where

$$F_{\mu\nu}(x) = \frac{1}{2ig} [C_{\mu\nu}(x) - C_{\mu\nu}^\dagger(x)], \quad (83)$$

and  $C_{\mu\nu}(x)$  is the  $1 \times 1$  clover term. We denote the integrated topological charge as  $Q$ , where

$$Q = \sum_x q(x). \quad (84)$$

Both the action and the topological charge densities appear invariant with only a few pixels in each respective image changing. This is reflected in the near-perfect correlation between the initial and precondition densities for both the action ( $C_{IP}^S = 0.99986$ ) and topological charge ( $C_{IP}^q = 0.99870$ ), where



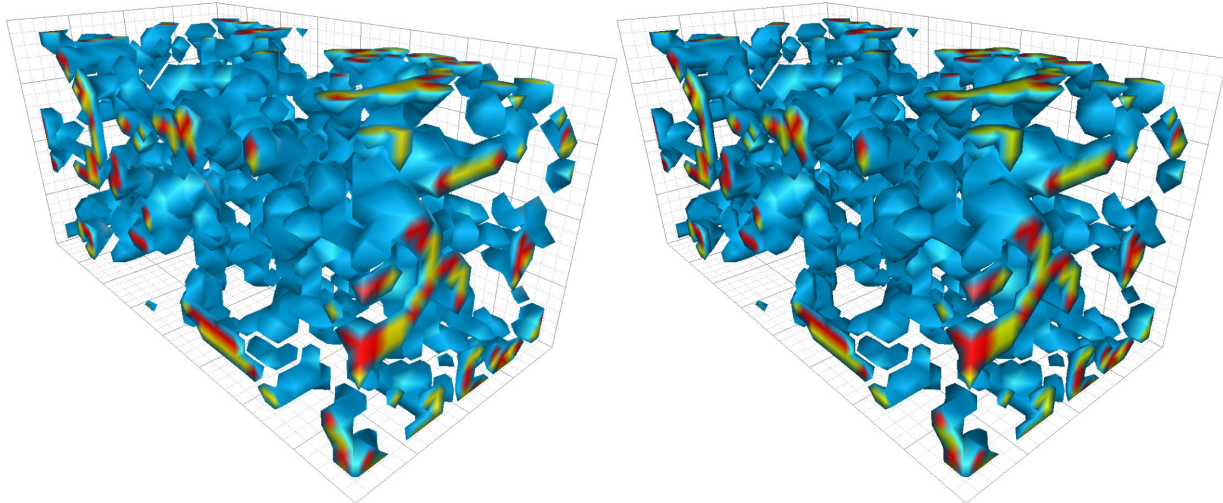


FIG. 3. Action density  $S(x)$  of a single time slice of a  $Z(3)$  center-vortex gauge field before (left) and after (right) centrifuge preconditioning at  $\omega = 0.02$ . The initial mean action density  $\langle S_I \rangle = 0.046859$ , the preconditioned mean action density  $\langle S_P \rangle = 0.049082$ , and the correlation of the respective action densities  $C_{IP}^S = 0.99986$ .

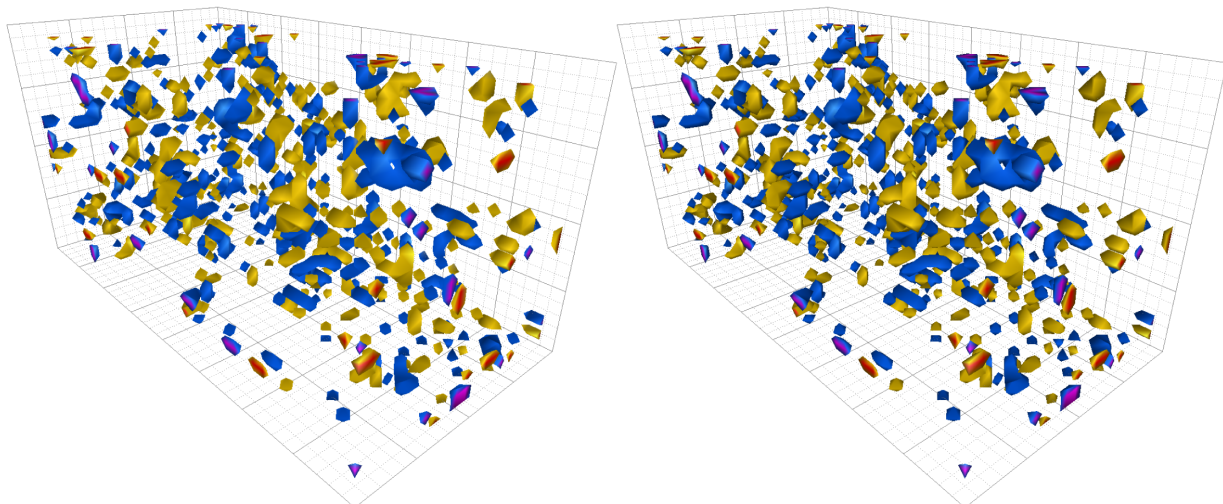


FIG. 4. Topological charge density  $q(x)$  of a single time slice of a  $Z(3)$  center-vortex gauge field before (left) and after (right) centrifuge preconditioning at  $\omega = 0.02$ . The initial integrated topological charge  $Q_I = 0.75282$ , the preconditioned integrated topological charge  $Q_P = 0.76792$ , and the correlation of the respective topological charge densities  $C_{IP}^q = 0.99870$ .

$$C_{IP}^S = \frac{\langle S_I(x)S_P(x) \rangle}{\sqrt{\langle S_I^2(x) \rangle} \sqrt{\langle S_P^2(x) \rangle}}, \quad (85)$$

$$C_{IP}^q = \frac{\langle q_I(x)q_P(x) \rangle}{\sqrt{\langle q_I^2(x) \rangle} \sqrt{\langle q_P^2(x) \rangle}}, \quad (86)$$

and the subscripts  $I$  and  $P$  denote *initial* and *preconditioned*, respectively. This suggests that we have successfully broken the diagonal symmetry without significantly altering the underlying center-vortex structure of the gauge field.

In general, we would consider the topological charge density to have physical meaning when the gauge field is smooth enough for the Atiyah-Singer index theorem to be satisfied [56], such that the gluonic definition of the integrated topological charge is approximately an integer and also agrees with the fermionic definition measured by the difference of left- and right-handed zero modes of the overlap-Dirac operator [57]. Previous studies show that two to three sweeps of standard stout-link smoothing at  $\rho = 0.1$  is required for the lattice operators to become good approximations to the physical charge [58–60]. The extremely rough nature of the projected vortex fields do not satisfy this condition. However, we do note that on a



center-vortex field, the topological charge density necessarily correlates with the singular points of the dual vortices [61] and that after, smoothing vortex fields can generate instantonlike structures [23]. Hence, the topological charge density remains of interest.

### A. Smoothness condition

As a measure of smoothness, we compare the mean densities of the standard Wilson action and the reconstructed Wilson action [62], given by

$$\langle S \rangle = \frac{1}{n_{\text{lat}}} \sum_x S(x), \quad (87)$$

and

$$\langle S_R \rangle = \frac{\beta}{2n_c n_d (n_d - 1)} \frac{1}{n_{\text{lat}}} \sum_{x,\mu,\nu} \text{Tr}[F_{\mu\nu}(x)F_{\mu\nu}(x)], \quad (88)$$

respectively.

The standard and reconstructed Wilson actions differ by  $\mathcal{O}(a^6)$  terms and perturbative renormalization factors. As the gauge field becomes smoother, the perturbative contributions are suppressed, and the renormalization factors tend toward 1. Thus, the difference between the standard and reconstructed action can be used as a measure of the smoothness of the gauge field. We consider the gauge field sufficiently smoothed when  $\langle S \rangle \approx \langle S_R \rangle$ .

### B. Smoothing in MCG

We examine centrifuge-preconditioned vortex fields that have been smoothed in MCG, starting with the Wilson flow. The Euler method for numerically integrating the Wilson flow [40] updates links according to

$$U_\mu(x, \tau) \rightarrow U_\mu(x, \tau + \epsilon) = e^{\epsilon Q_\mu(x)[U]} U_\mu(x, \tau). \quad (89)$$

In effect, this is an annealed implementation of stout-link smearing [39], where links are updated one at a time rather than simultaneously, and the smearing parameter  $\rho$  corresponds to the integration step size  $\epsilon$ . It follows then that flow time  $\tau = n\rho$  after  $n$  sweeps of smearing. While more sophisticated Runge-Kutta methods exist and have been used, we restrict our initial investigation to the Euler method.

Figure 5 shows the mean densities  $\langle S \rangle$  and  $\langle S_R \rangle$  of the centrifugal preconditioned gauge field as a function of Wilson flow time  $\tau$  computed with Euler integration step sizes  $\epsilon = 0.06, 0.02, 0.01, 0.005$ . The flow is no longer invariant and smooths the gauge field; however, the direct smearing of centrifuge preconditioned vortex fields is insufficient to bring  $\langle S \rangle$  and  $\langle S_R \rangle$  into agreement. The field remains rough and does not satisfy the smoothness condition above, required for the overlap-Dirac operator to be well-defined.

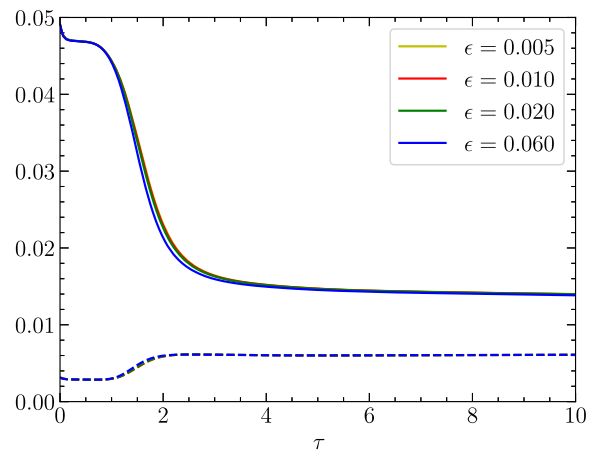


FIG. 5.  $\langle S \rangle$  (solid) and  $\langle S_R \rangle$  (dashed) as a function of Wilson flow time  $\tau$  for integration step size  $\epsilon = 0.005, 0.01, 0.02, 0.06$ .

In the spirit of gradient flow, we now turn to annealed  $U$ -link smearing (AUS) with small  $\alpha = 0.02$ . As mentioned previously, AUS is identical in form to APE smearing, but the links are effectively updated one at a time rather than simultaneously. We employ the overimprovement formalism where the staples term is given in Eq. (53). We choose  $\epsilon = -0.25$  as per Ref. [48]. We can consider AUS coupled with either unit circle projection (AUS + UCP) or MaxReTr reuniterization (AUS + MaxReTr).

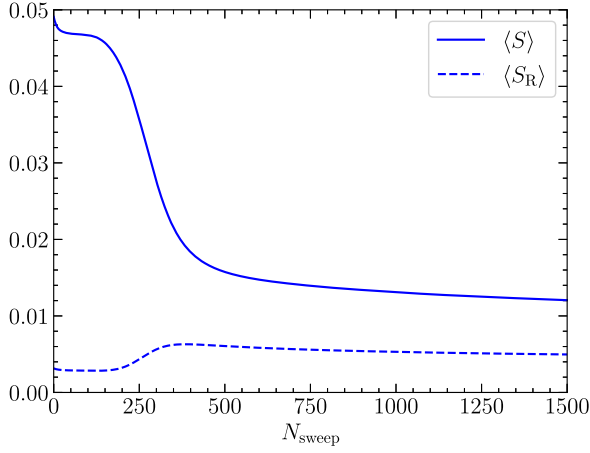
Figure 6(a) shows the results for AUS with unit circle projection. Again, (as with the Wilson flow above) on centrifugal preconditioned vortex fields, the gauge field is smoothed but insufficiently to bring  $\langle S \rangle$  and  $\langle S_R \rangle$  into agreement and satisfy the required smoothness condition. We find similar results in Fig. 6(b) where the MaxReTr reuniterization has been used instead.

In all three of the cases above, the smeared links remain diagonal. This is in some sense expected, as taking a linear combination of the diagonal matrices will result in a diagonal matrix for the staples, such that the smoothed link will also remain within the diagonal subgroup of  $SU(3)$ . This means that the smoothing process is unable to form links that encompass the full manifold of the special unitary group.

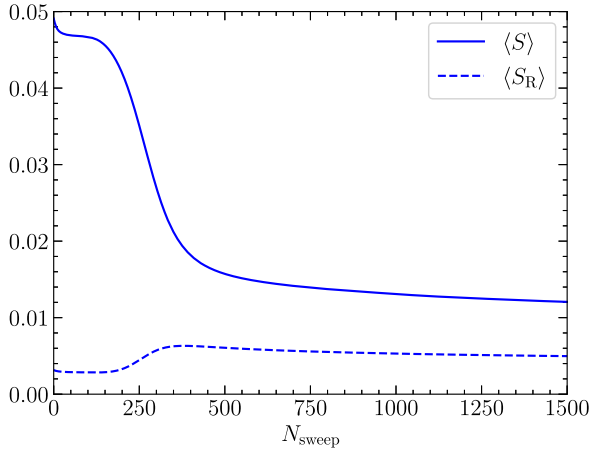
The inability of these algorithms to smear the diagonal elements of a particular link into its off-diagonal elements appears to present a fundamental limitation to the amount of smoothing that can be achieved. As such, it seems necessary to employ an algorithm that is able to mix the diagonal and nondiagonal elements of a link. To this end, rather than starting from maximal center gauge, we consider the addition of a random gauge transformation.

### C. Smoothing in random gauge

The Wilson flow and AUS with unit circle projection are gauge equivariant, which is to say for some smoothing process  $\mathcal{S}$  and gauge transformation,



(a) Unit circle projection.



(b) MaxReTr reunitarisation.

FIG. 6.  $\langle S \rangle$  and  $\langle S_R \rangle$  as a function of  $N_{\text{sweep}}$  iterations of overimproved AUS at  $\epsilon = -0.25$  and  $\omega = 0.02$  using (a) unit circle projection and (b) MaxReTr reunitarization, applied to a centrifuge preconditioned gauge field.

$$U_\mu(x) \rightarrow U_\mu^G(x) = G(x)U_\mu(x)G^\dagger(x + \hat{\mu}), \quad (90)$$

that

$$\mathcal{S}\{U_\mu^G(x)\} = G(x)\mathcal{S}\{U_\mu(x)\}G^\dagger(x + \hat{\mu}). \quad (91)$$

As the linear combination of two diagonal matrices remains diagonal, this gauge equivariance prevents the analytic smoothing algorithms from leaving the diagonal subgroup of  $SU(3)$ . This is not the case in general for AUS with MaxReTr reunitarization. As such, we repeat the AUS + MaxReTr calculation with identical parameters, but this time, we have transformed the centrifuge preconditioned gauge field to a random gauge before smoothing. We see in Fig. 7 that now, the gauge field can be sufficiently smoothed, achieving agreement between the action and reconstructed action with enough ( $N_{\text{sweeps}} > 1000$ ) sweeps

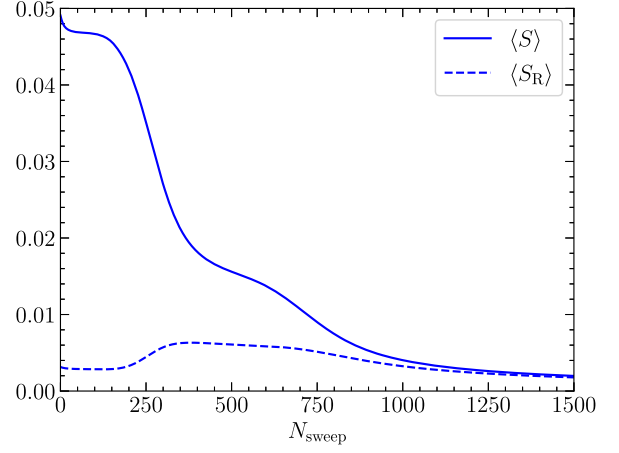


FIG. 7.  $\langle S \rangle$  and  $\langle S_R \rangle$  as a function of  $N_{\text{sweep}}$  iterations of overimproved AUS at  $\epsilon = -0.25$  and  $\omega = 0.02$  using the MaxReTr reunitarization applied to a centrifuge preconditioned gauge field that has been transformed to a random gauge.

of smoothing. We find that this smoothness condition is sufficient for the overlap-Dirac operator to be well-defined.

## VI. VORTEX-PRESERVED ANNEALING

One of the stated goals of finding a method to smooth center-vortex gauge fields was to preserve the underlying vortex structure. To this end, we introduce *vortex-preserved annealed smoothing* (VPAS) via an additional accept or reject step, which, in principle, can be applied to any iterative smoothing algorithm.

Let us first consider VPAS applied to center vortices in MCG. The AUS algorithm is run as usual to produce a candidate link in  $SU(3)$ ,

$$Z'_\mu(x) = \mathcal{P}_{SU(3)}\{V_\mu^{(n)}(x)\}. \quad (92)$$

The updated link is then given by

$$Z_\mu^{(n+1)}(x) = \begin{cases} Z'_\mu(x) & \text{if } \mathcal{P}_{Z(3)}\{Z'_\mu(x)\} = Z_\mu(x), \\ Z_\mu^{(n)}(x) & \text{otherwise,} \end{cases} \quad (93)$$

which is to say a candidate link is only accepted if it projects back to the original center-vortex link using Eq. (3). In the case where the original center-vortex link has undergone an arbitrary gauge transformation,

$$Z_\mu(x) \rightarrow G(x)Z_\mu(x)G^\dagger(x + \hat{\mu}), \quad (94)$$

the acceptance condition becomes

$$\mathcal{P}_{Z(3)}\{G^\dagger(x)Z'_\mu(x)G(x + \hat{\mu})\} = Z_\mu(x), \quad (95)$$

where the inverse of the original gauge transformation is applied to the candidate link. Note that in either case,

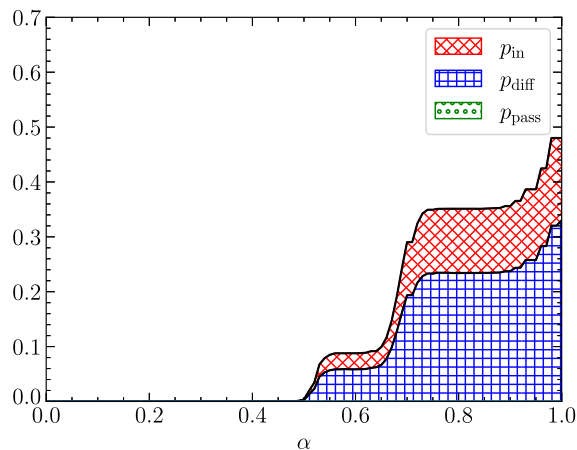


FIG. 8. The proportion of all possible combinations of links, weighted by multiplicity, which satisfy  $|\phi| > \frac{\pi}{2}$  ( $p_{\text{in}}$ ),  $Z_{\mu}^{(1)}(x) \neq Z_{\mu}(x)$  ( $p_{\text{diff}}$ ), and pass the vortex preservation step given  $Z_{\mu}^{(1)}(x) \neq Z_{\mu}(x)$  ( $p_{\text{pass}}$ ). Note  $p_{\text{pass}} = 0$  for all  $\alpha$ .

the  $Z(3)$  projection test is performed directly without reasserting the MCG condition in Eq. (2).

We now consider how VPAS with MaxReTr reunitarization applies to  $Z(3)$  center-vortex gauge field configurations by studying the outcome of the first sweep. We first examine the MCG case, where no centrifuge preconditioning has been applied. We study three quantities in our analysis:

- (i)  $p_{\text{in}}$  ( $n_{\text{in}}$ ), the proportion (absolute number) of links that satisfy  $|\phi| > \frac{\pi}{2}$  (required to perturb the vortex link),
- (ii)  $p_{\text{diff}}$  ( $n_{\text{diff}}$ ), the proportion (absolute number) of links for which  $Z_{\mu}^{(1)}(x) \neq Z_{\mu}(x)$  (accounting for the possibility that although the  $\phi$  condition is satisfied, it is still possible the projected link could be the same as the original), and
- (iii)  $p_{\text{pass}}$  ( $n_{\text{pass}}$ ), the proportion (absolute number) of candidate links that pass the vortex preservation step, given  $Z_{\mu}^{(1)}(x) \neq Z_{\mu}(x)$ .

These definitions necessitate the condition  $p_{\text{in}} \geq p_{\text{diff}} \geq p_{\text{pass}}$  holds.<sup>1</sup>

In Fig. 8, we compute these values for all combination of links, once again in the  $\beta \rightarrow 0$  limit where a given link has an equal probability to be one of the three center phases and weight each combination by its multiplicity. Most strikingly,  $p_{\text{pass}} = 0$  for all values of  $\alpha$ . This implies that if the updated link is different from the original, the phase of its trace will always fall outside the sector, which center projects to the original link.

We repeat this analysis on a true  $Z(3)$  projected gauge field configuration. The proportions are presented in Fig. 9,

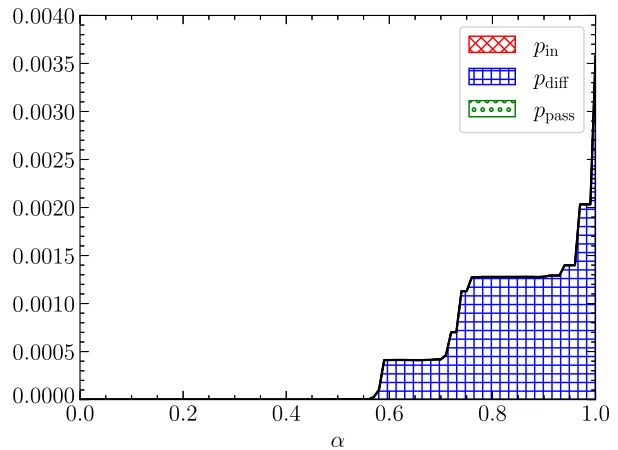


FIG. 9. The proportion of links of a  $Z(3)$  pure gauge field configuration, which satisfy  $|\phi| > \frac{\pi}{2}$  ( $p_{\text{in}}$ ),  $Z_{\mu}^{(1)}(x) \neq Z_{\mu}(x)$  ( $p_{\text{diff}}$ ), and pass the vortex preservation step given  $Z_{\mu}^{(1)}(x) \neq Z_{\mu}(x)$  ( $p_{\text{pass}}$ ). Note  $p_{\text{pass}} = 0$  for all  $\alpha$  and  $p_{\text{in}} = p_{\text{diff}}$  for all  $\alpha < 1$ .

while the absolute values are tabulated at intervals of 0.1 for  $\alpha$  in Table I. Consistent with the analysis presented in Fig 8, we see  $p_{\text{pass}} = 0$  for all values of  $\alpha$  and similar shaped curves for  $p_{\text{diff}}(\alpha)$ . However, unlike the previous analysis, we have that  $p_{\text{in}} = p_{\text{diff}}$  for all  $\alpha$ .

The same analysis is performed after centrifuge preconditioning and presented in Fig. 10 and Table II, where  $p_{\text{in}}$  has been dropped as this condition only applies to an unconditioned  $Z(3)$  gauge field where all links are proportional to the identity. Here (aside from the trivial  $\alpha = 0$  case), we see not only that every updated link is different from the original at all values of  $\alpha$ , but also that every candidate link passes the vortex preservation step below  $\alpha \approx 0.5$  and almost all ( $> 99.5\%$ ) at larger values of  $\alpha$ .

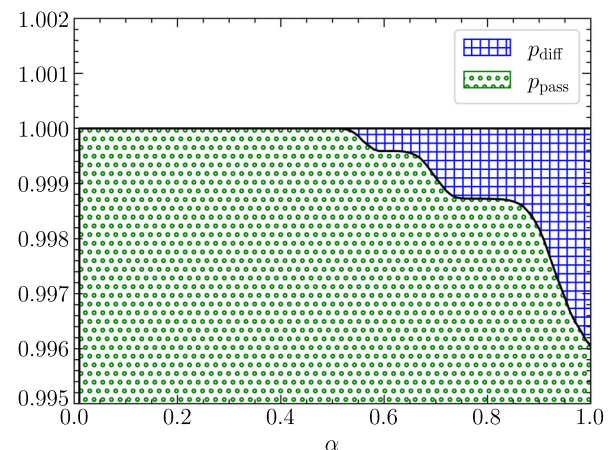
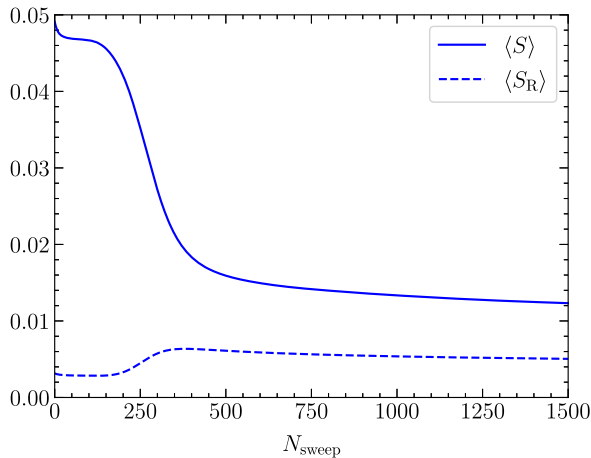


FIG. 10. The proportion of links of a centrifuge preconditioned  $Z(3)$  pure gauge field configuration, which satisfy  $Z_{\mu}^{(1)}(x) \neq Z_{\mu}(x)$  ( $p_{\text{diff}}$ ), and pass the vortex preservation step given  $Z_{\mu}^{(1)}(x) \neq Z_{\mu}(x)$  ( $p_{\text{pass}}$ ). Note that  $p_{\text{in}} = 1$  for all  $\alpha$ .

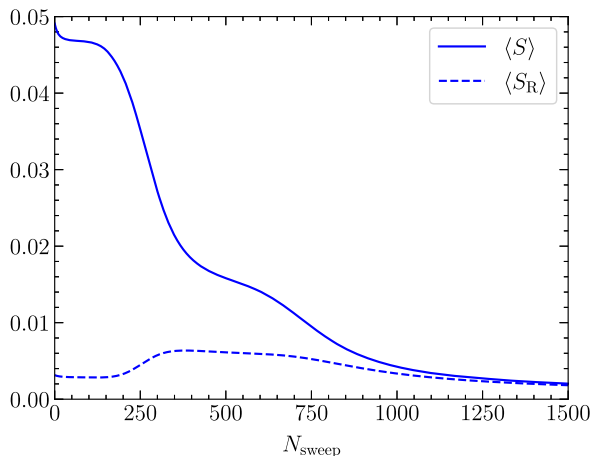
<sup>1</sup>See Sec. III A for an explanation of the apparent violation of this condition at  $\alpha = 1.0$  in Table I.

TABLE II. The number of links of a centrifuge preconditioned  $Z(3)$  pure gauge field configuration, which satisfy  $|\phi| > \frac{\pi}{2}$  ( $p_{\text{in}}$ ),  $Z_{\mu}^{(1)}(x) \neq Z_{\mu}(x)$  ( $p_{\text{diff}}$ ), and pass the vortex preservation step given  $Z_{\mu}^{(1)}(x) \neq Z_{\mu}(x)$  ( $p_{\text{pass}}$ ). The lattice has 1280000 links.

$\alpha$	$n_{\text{diff}}$	$n_{\text{pass}}$
0.1	1280000	1280000
0.2	1280000	1280000
0.3	1280000	1280000
0.4	1280000	1280000
0.5	1280000	1280000
0.6	1280000	1279473
0.7	1280000	1278853
0.8	1280000	1278363
0.9	1280000	1277673
1.0	1280000	1274937



(a) No random gauge transformation.



(b) Random gauge transformation.

FIG. 11.  $\langle S \rangle$  and  $\langle S_R \rangle$  as a function of  $N_{\text{sweep}}$  iterations of overimproved VPAS at  $\epsilon = -0.25$  and  $\omega = 0.02$  using the MaxReTr reunitization applied to a centrifuge preconditioned gauge field (a) without and (b) with a random gauge transformation applied after preconditioning and before smoothing.

While this suggests that a vortex-preservation step is not required for  $\alpha < 0.5$ , we note this is only for the first sweep following centrifugal preconditioning. Eventually, the vortex-preservation step does have an effect on the smoothing process.

Performing the same one-sweep analyses after a random gauge transform has been applied produces near-identical results and, for the sake of brevity, will not be presented herein. This is not unexpected, as we are only considering the first sweep. As we can see, comparing Figs. 6 and 7, the random gauge transformation only begins to have significance after several sweeps.

Applying VPAS with MaxReTr reunitization to a centrifuge preconditioned gauge field, we find similar results, presented in Fig. 11, to what we have seen with regular AUS. Once again, applying a random gauge transform to the field is necessary to achieve sufficient smoothing.

## VII. SMOOTHING METHOD COMPARISON

Throughout the previous sections, we have arrived at three viable smoothing methods for  $Z(3)$  center-vortex gauge fields. In Sec. II C, we showed that an APE-style smearing algorithm can only alter a  $Z(3)$  vortex field provided the smearing parameter  $\alpha$  is sufficiently large. Furthermore, in Sec. III, we found that the degree of smoothing was only sufficient if the vortex field had undergone a random gauge transformation and the MaxReTr reunitization was employed. Choosing also to employ the overimprovement formalism at  $\epsilon = -0.25$  with smearing parameter  $\alpha = 0.7$  and, implementing the algorithm in an annealed manner, we have arrived at our first smoothing recipe, which we denote throughout this section as AS for annealed smoothing.

In the spirit of approaching the gradient flow, we showed in Sec. V that the use of a small smearing parameter

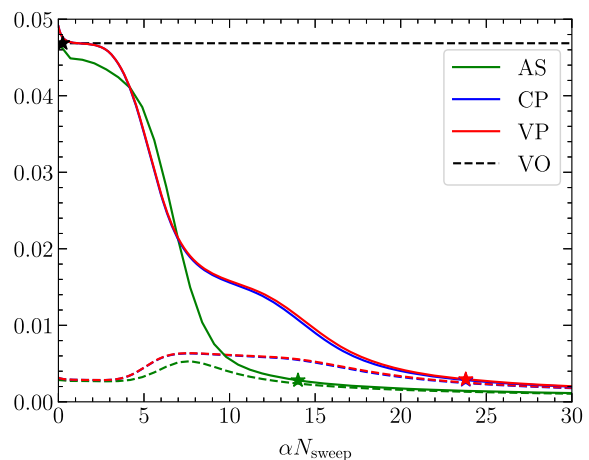


FIG. 12.  $\langle S \rangle$  (solid) and  $\langle S_R \rangle$  (dashed) as a function of  $\alpha N_{\text{sweep}}$  for each smoothing algorithm. The stars denote the number of sweeps chosen for algorithm comparison ( $N_{\text{sweep}} = 20$  for AS,  $N_{\text{sweep}} = 1190$  for CP and VP).



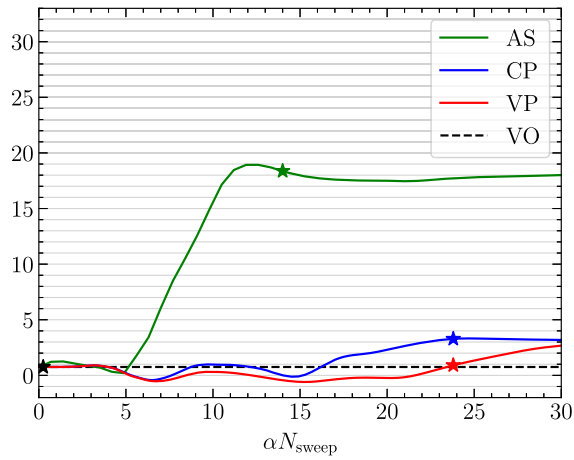


FIG. 13. Integrated topological charge  $Q$  as a function of  $\alpha N_{\text{sweep}}$  for each smoothing algorithm. The stars denote the number of sweeps chosen for algorithm comparison ( $N_{\text{sweep}} = 20$  for AS,  $N_{\text{sweep}} = 1190$  for CP and VP).

TABLE III. Summary of smoothing recipes. Steps are applied from left to right starting with the  $Z(3)$  center-vortex configuration in MCG.  $C$  indicates centrifuge preconditioning with rotation angle  $\omega$ .  $R$  indicates the application of a random gauge transformation.  $N_{\text{AUS}}$  indicates the number of sweeps of AUS with smearing parameter  $\alpha$ .  $V$  indicates if a vortex-preservation step was included in the AUS smearing.

Algorithm	$C$	$\omega$	$R$	$N_{\text{AUS}}$	$\alpha$	$V$
VO	✗	...	✗	0	...	...
AS	✗	...	✓	20	0.7	✗
CP	✓	0.02	✓	1190	0.02	✗
VP	✓	0.02	✓	1190	0.02	✓

$\alpha < \alpha_{\text{min}}$  is enabled by centrifuge preconditioning the vortex field. A random gauge transformation is necessarily applied after preconditioning to achieve the required level of smoothing to define our second recipe, which we denoted as CP for centrifuge preconditioning. We choose an AUS smearing parameter of  $\alpha = 0.02$  applied to a

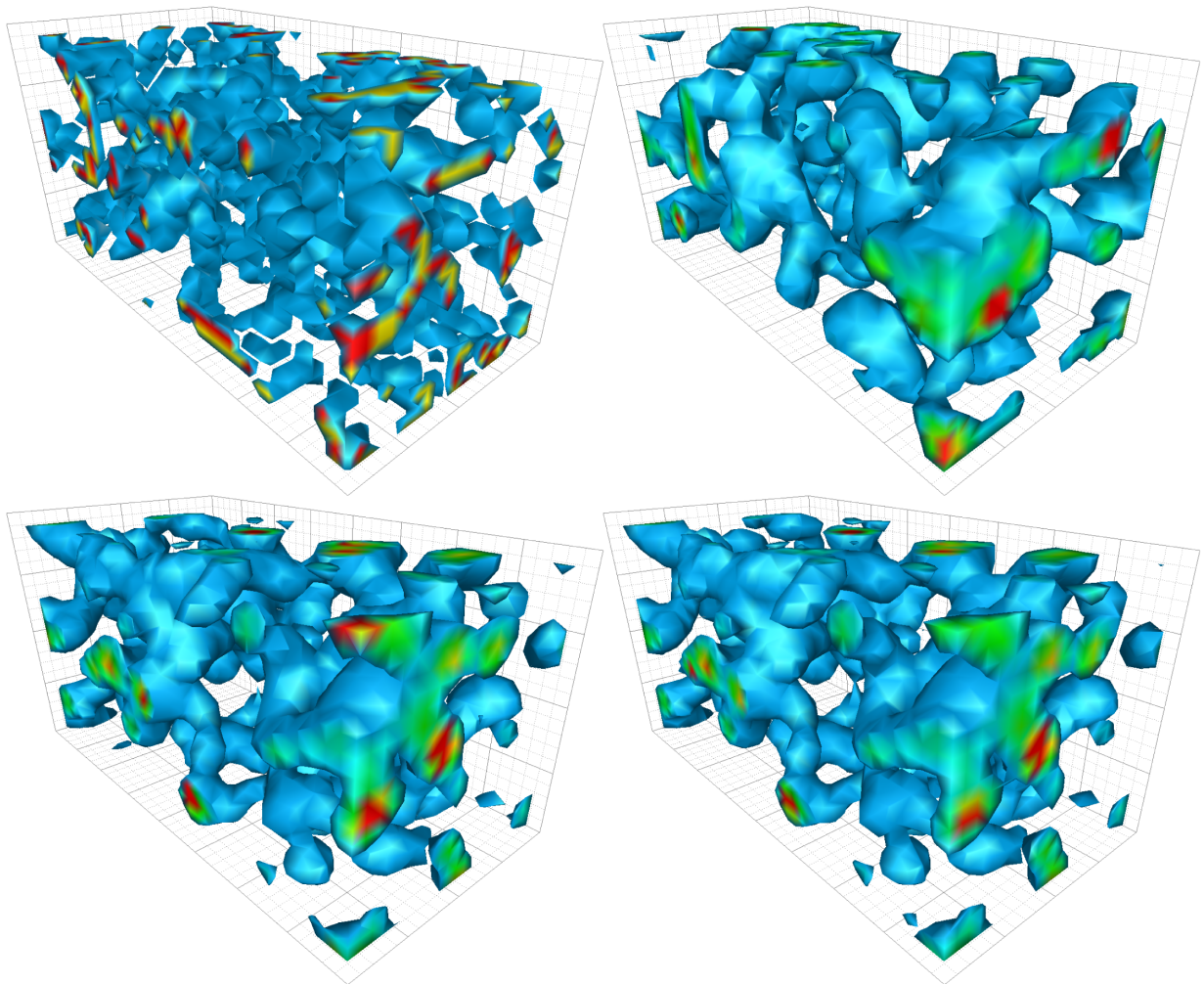


FIG. 14. Action density of a single time slice after smoothing. Clockwise from top left: VO, AS, CP, VP.



TABLE IV. The correlation  $C_{XY}^S$  of action densities  $S_X(x)$  and  $S_Y(x)$  of the gauge fields after respective smoothing algorithms  $X$  and  $Y$  have been applied.

	VO	AS	CP	VP
VO	1.000	0.397	0.397	0.404
AS	...	1.000	0.518	0.512
CP	...	...	1.000	0.943
VP	...	...	...	1.000

random gauge transformed, centrifuge preconditioned gauge field with rotation angle  $\omega = 0.02$ . Finally, in our third recipe, denoted VP for vortex preservation, we include the vortex preservation step in what is otherwise identical to our second recipe.

In addition to the resultant gauge fields of each smoothing recipe, we also consider the original  $Z(3)$  gauge field (denoted VO for vortex-only) without any smoothing as a reference.

In summary, we have four gauge fields to compare:

VO original vortex-projected gauge field,  
 AS large  $\alpha$ , APE-style, random-gauge-transformed annealed smoothing,  
 CP as for AS except with small  $\alpha$  and centrifuge preconditioning,  
 VP as for CP but with vortex preservation step applied.

We present the mean action  $\langle S \rangle$  and reconstructed action  $\langle S_R \rangle$  densities for each algorithm as a function of  $\alpha N_{\text{sweep}}$  in Fig. 12. Similarly, in Fig. 13, we present the integrated topological charge  $Q$  for each algorithm as a function of  $\alpha N_{\text{sweep}}$ . The reference value for the vortex-only field (without any smoothing) is represented as a dashed horizontal line.

The trajectories of the mean action density for CP and VP are nearly identical, so as to be almost indistinguishable for the majority of the smoothing trajectory. A more detailed analysis is necessary to elucidate any subtle differences that exist between the respective algorithms. Meanwhile, the trajectory for AS is roughly proportionate

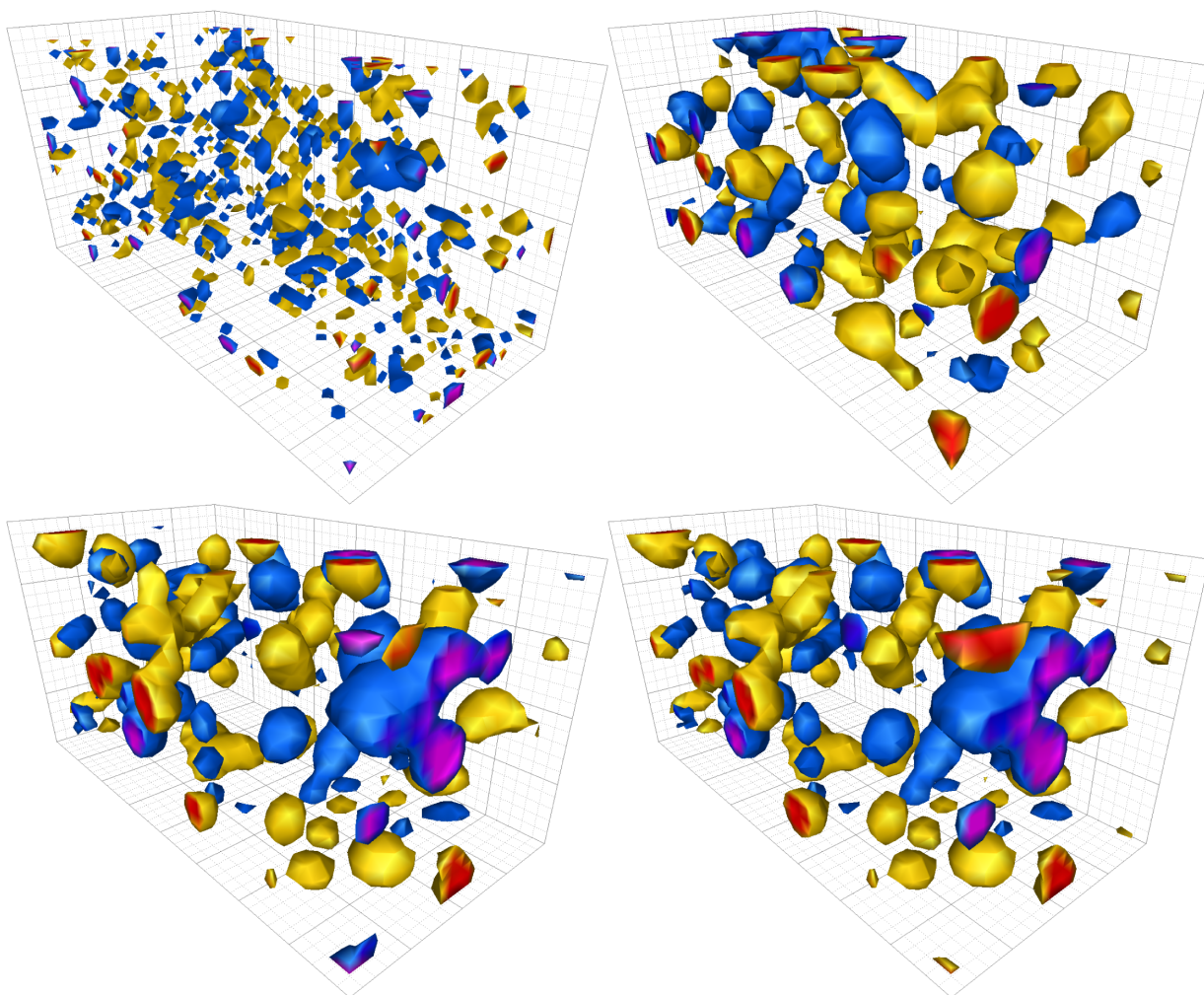


FIG. 15. Topological charge density of a single time slice after smoothing. Clockwise from top left: VO, AS, CP, VP.

to the  $CP$ , and  $VP$  curves for  $\alpha N_{\text{sweep}} < 6$  but diverges rapidly above that threshold.

The difference between the large- $\alpha$  AS algorithm and the small- $\alpha$   $CP$  and  $VP$  algorithms is most apparent in the trajectories of the integrated topological charge.  $CP$  and  $VP$  track relatively closely, with a small divergence from  $\alpha N_{\text{sweep}} \sim 7$ , after which, they appear to be converging on the same integer value by  $\alpha N_{\text{sweep}} \sim 30$ . By contrast, the AS trajectory acutely diverges from the  $CP$  and  $VP$  curves at around  $\alpha N_{\text{sweep}} \sim 5$ .

In order to perform a more detailed analysis, we choose a fixed number of AUS sweeps for each algorithm (20 for AS, and 1190 for  $CP$  and  $VP$ ) as a point of comparison, such that the different gauge fields have approximately matched total actions. The respective number of sweeps chosen for each algorithm are marked by stars in Figs. 12 and 13. See Table III for a summary of each algorithm in the context of the following discussion.

We present visualizations of the respective action densities in Fig. 14 and compute their correlations where  $C_{XY}^S$  given by

$$C_{XY}^S = \frac{\langle S_X(x)S_Y(x) \rangle}{\sqrt{\langle S_X^2(x) \rangle} \sqrt{\langle S_Y^2(x) \rangle}}, \quad (96)$$

is the correlation between  $S_X(x)$  and  $S_Y(x)$  for respective smearing processes  $X$  and  $Y$ . These are presented in Table IV.

Similarly, we present visualizations of the respective topological charge densities in Fig. 15 and compute their correlations where  $C_{XY}^q$ , given by

$$C_{XY}^q = \frac{\langle q_X(x)q_Y(x) \rangle}{\sqrt{\langle q_X^2(x) \rangle} \sqrt{\langle q_Y^2(x) \rangle}}, \quad (97)$$

is the correlation between  $q_X(x)$  and  $q_Y(x)$  for respective smearing processes  $X$  and  $Y$ . These are presented in Table V.

The superior similarity of the  $CP$  and  $VP$  action densities to the original vortex field evident in the visualizations, as compared to AS, indicates not only that the use of a small smearing parameter is desirable, but it is fundamentally important in preserving the underlying vortex structure. With regard to the action density, the numerical correlation

TABLE V. The correlation  $C_{XY}^q$  of topological charge densities  $q_X(x)$  and  $q_Y(x)$  of the gauge fields after respective smoothing algorithms  $X$  and  $Y$  have been applied.

	VO	AS	CP	VP
VO	1.000	0.010	-0.001	0.002
AS	...	1.000	0.009	0.000
CP	...	...	1.000	0.886
VP	...	...	...	1.000

of  $VP$  with the original vortex field is slightly higher (by  $\sim 2\%$ ) as compared to AS and  $CP$ .

Visually, the topological charge density for VO is qualitatively different from the three smoothed fields in terms of the size and number of objects. The numerical comparison of the topological charge densities indicates they are essentially uncorrelated, with the exception of  $CP$  and  $VP$ , which do show a strong positive numerical correlation and similarity in their visualisations.

## VIII. SUMMARY

Throughout this work, we have studied the application of a variety of  $SU(3)$  gauge field smoothing methods to  $Z(3)$  center-vortex gauge fields, with an aim to achieve sufficient smoothness so as to be able to meaningfully evaluate the overlap-Dirac operator. An additional aim is to preserve (as much as possible) the original vortex structure identified in MCG. Due to the proportionality of the vortex-field links to the identity, a naive application of traditional smoothing algorithms is either ineffectual or limited, containing subtle issues that are not obviously manifest.

To overcome these issues, we introduced a novel method, centrifuge preconditioning, which perturbs the center elements from  $Z(3)$  into the  $U(1) \times U(1) \times Z(3)$  diagonal subgroup of  $SU(3)$ . The centrifuge preconditioning step is constructed in a manner that breaks the proportionality of the links to the identity while preserving the original vortex information.

Agreement between the action and reconstructed action is set as the condition for sufficient smoothness in order to employ overlap fermions on the smoothed vortex field. The amount of smoothing that can be obtained with analytic methods is fundamentally limited by the gauge equivariant property of these methods, which, even with centrifuge preconditioning, remain within the diagonal subgroup of  $SU(3)$  (up to a gauge transformation).

It is only through the application of a random gauge transform together with the MaxReTr reunitarization—an update-based method that is not gauge equivariant—as part of an APE-based annealed smoothing formalism, that it becomes possible to depart from the diagonal subgroup and expand the smoothed links to the greater part of the  $SU(3)$  group manifold.

Additional to centrifuge preconditioning, to preserve the vortex structure throughout the annealed smoothing process, the concept of a vortex preservation step was introduced. This consists of an accept or reject step within the annealed smoothing process, where the update for a given link is only accepted if the argument of the trace projects to the same  $Z(3)$  element as the center phase identified in the MCG of the original gauge field.

Based on the above, three smoothing recipes were formulated (AS,  $CP$ ,  $VP$ ), which, along with the pure vortex field (VO), were compared (refer to Table III for

a summary). With regard to the action density, the visualizations in Fig. 14 show the  $CP$  and  $VP$  algorithms produce action densities resembling the original vortex structure. Considering the quantitative measure of Eq. (96), all three smoothing recipes were found to have a similar correlation with the original field, with  $VP$  having the highest of the three by a small margin. On such rough fields, the microscopic structure of the topological charge density appears to be volatile, and as a result, there is essentially no correlation between three of the four fields examined. The exceptional pair is  $CP$  and  $VP$ , which produce highly correlated topological charge densities, the only difference between these two recipes being that  $VP$  includes the vortex-preserved annealing step, ensuring that the argument of the trace of the links projects to the original center element.

The conclusion is that the centrifuge preconditioning and vortex-preserved annealing techniques enable the successful smoothing of vortex fields and will be studied further in future work.

### ACKNOWLEDGMENTS

We thank the PACS-CS Collaboration for making their configurations available via the International Lattice Data Grid (ILDG). This research was undertaken with resources provided by the Pawsey Supercomputing Centre through the National Computational Merit Allocation Scheme with funding from the Australian Government and the Government of Western Australia. Additional resources were provided from the National Computational Infrastructure (NCI) supported by the Australian Government through Grant No. LE190100021 via the University of Adelaide Partner Share. This research is supported by Australian Research Council through Grants No. DP190102215 and DP210103706. W. K. is supported by the Pawsey Supercomputing Centre through the Pawsey Centre for Extreme Scale Readiness (PaCER) program.

### APPENDIX A: GENERATORS OF SU(3)

The eight traceless anti-Hermitian matrices  $T^a$  are the generators of SU(3) and are proportional to the Gell-Mann matrices. We choose the normalization condition  $\text{Tr}[T^a T^b] = -\frac{1}{2} \delta^{ab}$  to ensure the structure constants  $f^{abc}$  defined by  $[T^a, T^b] = f^{abc} T^c$  are real and totally antisymmetric in the indices.

Up to a center phase factor, the diagonal subgroup of SU(3) is spanned by the subset of generators  $\{T^3, T^8\}$ , where  $T^3$  and  $T^8$  are diagonal. We can write an element of the diagonal subgroup as

$$\exp\left(n \frac{2\pi i}{3}\right) \exp(a_3 T^3 + a_8 T^8), \quad (\text{A1})$$

where  $n \in \{-1, 0, 1\}$ , and  $a_3, a_8 \in \mathbb{R}$ . The subgroup is Abelian as  $[T^3, T^8] = 0$ , and it is straightforward to see that it is isomorphic to  $U(1) \times U(1) \times Z(3)$ .

### APPENDIX B: DERIVATION OF $\alpha_{\min}$ FOR MaxReTr REUNITERIZATION WITHIN THE OVERIMPROVEMENT FORMALISM

Without loss of generality, let  $Z_\mu(x) = \mathbb{1}$ . Hence,  $L^1$  from Eq. (55) becomes

$$L^1 = (1 - \alpha) + \frac{\alpha}{6} \Sigma_\mu^\dagger(x), \quad (\text{B1})$$

which, explicitly within the overimprovement formalism, is

$$L^1 = (1 - \alpha) + \frac{\alpha}{6} \left\{ \left( \frac{5 - 2\epsilon}{3} \right) S_\mu(x) + \left( \frac{\epsilon - 1}{12u_0^2} \right) R_\mu(x) \right\}, \quad (\text{B2})$$

where  $S_\mu(x)$  represents the three-link staple terms and  $R_\mu(x)$  represents the five-link rectangle terms in Eq. (53). We restrict the overimprovement term such that  $\epsilon \in [-\frac{5}{2}, 1]$  to ensure

$$\frac{5 - 2\epsilon}{3} \geq 0, \quad (\text{B3})$$

and

$$\frac{\epsilon - 1}{12u_0^2} \leq 0. \quad (\text{B4})$$

Then, the minima of the real component of  $L^1[\Sigma_\mu(x)]$  for a given  $\alpha$  occur when all six terms contributing to  $S_\mu(x)$  have nontrivial phase (and hence, a real component equal to  $-0.5$ ). Replacing any term with the identity necessarily increases the real component of  $S_\mu(x)$ . Hence, the values of  $S_\mu(x)$  for which the real component of  $L^1$  is minimized are given by

$$\begin{aligned} S_\mu(x) &= n e^{+i\frac{2\pi}{3}} + (6 - n) e^{-i\frac{2\pi}{3}} \\ &= 6 \cos\left(\frac{2\pi}{3}\right) + i(2n - 6) \sin\left(\frac{2\pi}{3}\right) \\ &= -3 + i(2n - 6) \sin\left(\frac{2\pi}{3}\right), \end{aligned} \quad (\text{B5})$$

where  $n \in [0, 6] \subset \mathbb{Z}$ . As we are not concerned with the imaginary component, for simplicity and without loss of generality, we take  $n = 3$  for which the imaginary component of  $S_\mu(x)$  vanishes. Evaluating  $S_\mu(x)$  for  $n = 3$ , we have  $S_\mu(x) = -3$ .

On the other hand, as the factor in front of  $R_\mu(x)$  is negative, the minima of  $L^1$  for a given  $\alpha$  occur when the real



component of  $R_\mu(x)$  is maximized. This occurs when all 18 loops contributing to  $R_\mu(x)$  are the identity with real component equal to 1. Replacing any term with one that has a nontrivial phase (and hence, a real component equal to  $-0.5$ ) necessarily reduces the real component of  $R_\mu(x)$ . Hence, the minima of  $L^1$  must occur when  $R_\mu(x) = 18$ .

Substituting into Eq. (B2), we have

$$L^1 = (1 - \alpha) + \frac{\alpha}{6} \left\{ \left( \frac{5 - 2\epsilon}{3} \right) (-3) + \left( \frac{\epsilon - 1}{12u_0^2} \right) (18) \right\}. \quad (\text{B6})$$

Recalling that we require  $\text{Re}L^1 < 0$ , and simplifying, we have

$$\begin{aligned} 0 &> (1 - \alpha) + \frac{\alpha}{6} \left\{ \left( \frac{5 - 2\epsilon}{3} \right) (-3) + \left( \frac{\epsilon - 1}{12u_0^2} \right) (18) \right\} \\ 0 &> 1 - \alpha + \alpha \left\{ \frac{2\epsilon - 5 + \frac{3}{2} \left( \frac{\epsilon - 1}{u_0^2} \right)}{6} \right\} \\ -1 &> \alpha \left\{ \frac{2\epsilon - 11 + \frac{3}{2} \left( \frac{\epsilon - 1}{u_0^2} \right)}{6} \right\} \\ \alpha &> \frac{-6}{2\epsilon - 11 + \frac{3}{2} \left( \frac{\epsilon - 1}{u_0^2} \right)}. \end{aligned} \quad (\text{B7})$$

Let  $\Sigma_\mu^{\min}(x)$  denote a staples term that minimizes the real component of  $L^1$  for  $Z_\mu(x) = \mathbb{1}$ . Then, for  $Z_\mu(x) = e^{\pm i\frac{2\pi}{3}}$ , the minima of the real component of  $L^1$  occur at  $e^{\mp i\frac{2\pi}{3}} \Sigma_\mu^{\min}(x)$ , and the same derivation follows.

- 
- [1] G. 't Hooft, *Nucl. Phys.* **B138**, 1 (1978).  
[2] G. 't Hooft, *Nucl. Phys.* **B153**, 141 (1979).  
[3] L. Del Debbio, M. Faber, J. Greensite, and S. Olejnik, *Phys. Rev. D* **55**, 2298 (1997).  
[4] M. Faber, J. Greensite, and S. Olejnik, *Phys. Rev. D* **57**, 2603 (1998).  
[5] L. Del Debbio, M. Faber, J. Giedt, J. Greensite, and S. Olejnik, *Phys. Rev. D* **58**, 094501 (1998).  
[6] R. Bertle, M. Faber, J. Greensite, and S. Olejnik, *J. High Energy Phys.* 03 (1999) 019.  
[7] M. Faber, J. Greensite, S. Olejnik, and D. Yamada, *J. High Energy Phys.* 12 (1999) 012.  
[8] M. Engelhardt, K. Langfeld, H. Reinhardt, and O. Tennert, *Phys. Rev. D* **61**, 054504 (2000).  
[9] M. Engelhardt and H. Reinhardt, *Nucl. Phys.* **B567**, 249 (2000).  
[10] M. Engelhardt, *Nucl. Phys.* **B585**, 614 (2000).  
[11] R. Bertle, M. Faber, J. Greensite, and S. Olejnik, *J. High Energy Phys.* 10 (2000) 007.  
[12] K. Langfeld, H. Reinhardt, and J. Gattnar, *Nucl. Phys.* **B621**, 131 (2002).  
[13] J. Greensite, *Prog. Part. Nucl. Phys.* **51**, 1 (2003).  
[14] F. Bruckmann and M. Engelhardt, *Phys. Rev. D* **68**, 105011 (2003).  
[15] M. Engelhardt, M. Quandt, and H. Reinhardt, *Nucl. Phys.* **B685**, 227 (2004).  
[16] P. Y. Boyko, V. G. Bornyakov, E. M. Ilgenfritz, A. V. Kovalenko, B. V. Martemyanov, M. Muller-Preussker, M. I. Polikarpov, and A. I. Veselov, *Nucl. Phys.* **B756**, 71 (2006).  
[17] E.-M. Ilgenfritz, K. Koller, Y. Koma, G. Schierholz, T. Streuer, V. Weinberg, and M. Quandt, *Proc. Sci. LATTICE2007* (2007) 311.  
[18] V. G. Bornyakov, E. M. Ilgenfritz, B. V. Martemyanov, S. M. Morozov, M. Muller-Preussker, and A. I. Veselov, *Phys. Rev. D* **77**, 074507 (2008).  
[19] A. O'Cais, W. Kamleh, K. Langfeld, B. Lasscock, D. Leinweber, P. Moran, A. Sternbeck, and L. von Smekal, *Phys. Rev. D* **82**, 114512 (2010).  
[20] M. Engelhardt, *Phys. Rev. D* **83**, 025015 (2011).  
[21] P. O. Bowman, K. Langfeld, D. B. Leinweber, A. Sternbeck, L. von Smekal, and A. G. Williams, *Phys. Rev. D* **84**, 034501 (2011).  
[22] E.-A. O'Malley, W. Kamleh, D. Leinweber, and P. Moran, *Phys. Rev. D* **86**, 054503 (2012).  
[23] A. Trewartha, W. Kamleh, and D. Leinweber, *Phys. Rev. D* **92**, 074507 (2015).  
[24] J. Greensite, *EPJ Web Conf.* **137**, 01009 (2017).  
[25] J. C. Biddle, W. Kamleh, and D. B. Leinweber, *Phys. Rev. D* **98**, 094504 (2018).  
[26] F. Spengler, M. Quandt, and H. Reinhardt, *Phys. Rev. D* **98**, 094508 (2018).  
[27] K. Langfeld, *Phys. Rev. D* **69**, 014503 (2004).  
[28] A. Montero, *Phys. Lett. B* **467**, 106 (1999).  
[29] M. Faber, J. Greensite, and S. Olejnik, *Phys. Lett. B* **474**, 177 (2000).  
[30] P. Hernandez, K. Jansen, and M. Luscher, *Nucl. Phys.* **B552**, 363 (1999).  
[31] D. H. Adams, *Phys. Rev. D* **68**, 065009 (2003).  
[32] H. Neuberger, *Phys. Rev. D* **61**, 085015 (2000).  
[33] W. Kamleh, D. H. Adams, D. B. Leinweber, and A. G. Williams, *Phys. Rev. D* **66**, 014501 (2002).  
[34] A. Trewartha, W. Kamleh, and D. Leinweber, *Phys. Lett. B* **747**, 373 (2015).  
[35] A. Trewartha, W. Kamleh, and D. B. Leinweber, *J. Phys. G* **44**, 125002 (2017).  
[36] K. Langfeld and E.-M. Ilgenfritz, *Nucl. Phys.* **B848**, 33 (2011).  
[37] R. Höllwieser and M. Engelhardt, *Phys. Rev. D* **92**, 034502 (2015).  
[38] F. D. R. Bonnet, P. Fitzhenry, D. B. Leinweber, M. R. Stanford, and A. G. Williams, *Phys. Rev. D* **62**, 094509 (2000).

- [39] C. Morningstar and M. Peardon, *Phys. Rev. D* **69**, 054501 (2004).
- [40] M. Lüscher, *Commun. Math. Phys.* **293**, 899 (2010).
- [41] M. Lüscher, *J. High Energy Phys.* 08 (2010) 071; 03 (2014) 092(E).
- [42] W. Kamleh, D. B. Leinweber, and A. G. Williams, *Phys. Rev. D* **70**, 014502 (2004).
- [43] S. Duane, A. D. Kennedy, B. J. Pendleton, and D. Roweth, *Phys. Lett. B* **195**, 216 (1987).
- [44] M. Falcioni, M. L. Paciello, G. Parisi, and B. Taglienti, *Nucl. Phys.* **B251**, 624 (1985).
- [45] M. Albanese *et al.*, *Phys. Lett. B* **192**, 163 (1987).
- [46] M. Garcia Perez, A. Gonzalez-Arroyo, J. R. Snippe, and P. van Baal, *Nucl. Phys.* **B413**, 535 (1994).
- [47] F. D. R. Bonnet, D. B. Leinweber, A. G. Williams, and J. M. Zanotti, *Phys. Rev. D* **65**, 114510 (2002).
- [48] P. J. Moran and D. B. Leinweber, *Phys. Rev. D* **77**, 094501 (2008).
- [49] N. Cabibbo and E. Marinari, *Phys. Lett.* **119B**, 387 (1982).
- [50] F. D. R. Bonnet, D. B. Leinweber, and A. G. Williams, *J. Comput. Phys.* **170**, 1 (2001).
- [51] B. Berg, *Phys. Lett.* **104B**, 475 (1981).
- [52] M. Teper, *Phys. Lett.* **162B**, 357 (1985).
- [53] M. Teper, *Phys. Lett. B* **171**, 81 (1986).
- [54] M. Teper, *Phys. Lett. B* **171**, 86 (1986).
- [55] E.-M. Ilgenfritz, M. L. Laursen, G. Schierholz, M. Muller-Preussker, and H. Schiller, *Nucl. Phys.* **B268**, 693 (1986).
- [56] M. F. Atiyah and I. M. Singer, *Ann. Math.* **87**, 484 (1968).
- [57] R. Narayanan and P. M. Vranas, *Nucl. Phys.* **B506**, 373 (1997).
- [58] P. J. Moran and D. B. Leinweber, *Phys. Rev. D* **78**, 054506 (2008).
- [59] P. J. Moran, D. B. Leinweber, and J. Zhang, *Phys. Lett. B* **695**, 337 (2011).
- [60] M. Teper, [arXiv:2202.02528](https://arxiv.org/abs/2202.02528).
- [61] J. C. Biddle, W. Kamleh, and D. B. Leinweber, *Phys. Rev. D* **102**, 034504 (2020).
- [62] S. O. Bilson-Thompson, D. B. Leinweber, and A. G. Williams, *Ann. Phys. (Amsterdam)* **304**, 1 (2003).